Control Oriented System Modelling and Instrumentation of Intelligent Walker-Human Systems

by

Halit Zengin

A thesis
presented to the University of Waterloo
in fulfillment of the
thesis requirement for the degree of
Master of Applied Science
in
Mechanical Engineering

Waterloo, Ontario, Canada, 2015

I hereby declare that I am the sole author of this thesis. This is a true copy of the thesis, including any required final revisions, as accepted by my examiners.

I understand that my thesis may be made electronically available to the public.

Abstract

Active intelligent walkers (i-walkers) are promising to provide stable and efficient motion to people with walking disabilities. There are three focuses in this thesis: system modelling, controller design, and instrumentation of an active type i-walker system considering interaction with human user as well. Two different control oriented system models and one high-fidelity model are proposed. All system models are designed as having two-body kinematics and consider the physical human-walker interaction (pHWI) based on the user gait dynamics and characteristics. The two-body kinematics of the systems define the relative motion of the user body with the i-walker. The dynamic models of control oriented systems are developed as single-body i-walker dynamics with human effect. These single-body models are classified as symmetric vs. asymmetric, and designed considering the vertical force components of pHWI on the i-walker. The symmetric model is developed for the center of gravity (CG) displacement of the i-walker human system only along the symmetric axis. The asymmetric model is more comprehensive than the symmetric one including the lateral CG displacement as well. The high-fidelity model considers the effect of human user as a separate dynamic body and covers the horizontal and vertical force components of pHWI during walking. Different control schemes are designed for each of the models with single-body dynamics, demonstrating the characteristics and efficiency of each model. All of these control designs are based on the same inverse kinematic controller, which utilizes two-body kinematic model and provides the desired i-walker velocities regarding the user motion intention. Each of the aforementioned dynamic controllers is designed to generate the torques required to track these desired velocities. Two different dynamic control schemes are proposed for dynamic controller: Proportional-integral-derivative (PID) and sliding mode controllers. The designed controllers are simulation tested in MATLAB/Simulink for the control oriented models. The asymmetric model parameters are also set for two different type of users with symmetric and asymmetric gait patterns, respectively. Finally, instrumentation of i-walkers for implementing the designed controllers is discussed, including presentation of a new human motion detection technique involving laser range finder (LRF) and encoders, and instrumentation is performed regarding the designed controllers.

Acknowledgements

I would like to express my deep sense of thanks and gratitude to my supervisor Dr. Baris Fidan for his great guidance, support, and respectable manner throughout my study. I would like to thank the review committee members, Dr. Nasser L. Azad and Dr. James Tung for their precious comments and suggestions.

I wish to dedicate my thesis to all my family, mom Semiha, my siblings Ibrahim and Suleyman, my grandmothers Fatma and Ayse, for their supports, prays, belief. I am so happy to have them. A special thank to my father Prof. Huseyin Zengin who has always been a role model for me with his dedication to his job.

I am privileged for having my dearest wife Nursefa Zengin. Without her continuous encouragement, support, patient and love, I would have never complete this study.

Many special thanks to my friends who have always supported and helped me in my tough times.

Table of Contents

List of Tables

List of Figures

List of Acronyms

CG	Center of Gravity
F/T	Force/Torque
I-walker	Intelligent Walker
LRF	Laser Range Finder
pHWI	physical Human Walker Interaction
PID	Proportional-Integral-Derivative
SMC	Sliding Mode Controller
WMR	Wheeled Mobile Robot

Chapter 1

Introduction

Everyone wishes to sustain an independent life, yet some pathologies, injuries, or age-related conditions cause partial/total loss of walking ability. The people in such conditions need assistance to perform daily living activities. However, insufficient caregiver services lead these people to use assistive support devices. Intelligent walkers (i-walkers) could have an important place among the mobility assistive devices, since they provide the opportunity of independent mobility for the people with walking impairments.

Different types of i-walker systems have been developed to assist people with walking difficulties. Due to safety concerns, the motion controllers of these systems have been designed as passive, i.e., producing only braking torque to the system in order to steer the i-walker. However, these passive systems increase the metabolic cost of the user and cause fatigue. Active i-walker systems are promising for addressing such issues and increasing walking efficiency. However, safety is still a fundamental problem for active systems due to two main reasons:

1) The unintentional movement of the i-walker.

2) Inappropriate torque generation since the load changes and center of gravity (CG) displacements in the i-walker system due to the physical human-walker interaction (pHWI) have not been considered.

We propose solutions to deal with these issues and aims at improving both the safety

and efficiency of human-walker mobility. Unlike the previous studies, this thesis focuses on control of an active type nonholonomic i-walker system considering pHWI based on the user gait dynamics and characteristics.

In this thesis, three different system models for the i-walker human system are proposed: two control oriented models and one high-fidelity model. All of these three models are based on two-body kinematics and take pHWI based on the user gait dynamics into consideration. The two-body kinematics for these systems are used to figure out the relative motion of the human torso with the i-walker. This relative motion is described as user motion intention. The two control oriented models are assumed to be single-body i-walker dynamics with human effect. These models with single-body dynamics are classified as symmetric vs. asymmetric and designed considering the vertical force components of pHWI during motion. The model with symmetric dynamics is designed based on the assumption that the location of i-walker CG changes along the symmetric axis of the i-walker in parallel with the user gait phase. The asymmetric model is developed to include CG displacement along lateral axis, and allows to model and users having different characteristics, e.g., users with symmetric or asymmetric gait patterns. The high-fidelity model proposed for detailed modelling and simulation of i-walker guided human-walker systems. Unlike first two models, this comprehensive model has two-body dynamics and designed inspiring from articulated frame steering vehicles. This multi-body approach allows to examine both vertical and horizontal force components of the pHWI during walking.

After deriving system models, two different control schemes are applied for each proposed control oriented system model demonstrating the characteristic and efficiency of these models. In this regard, an inverse two-body kinematic controller is implemented for both system models to produce the desired i-walker wheel positions and velocities based on the human motion intention which is defined as the relative motion of the user torso with the i-walker. Then, the i-walker systems are controlled by dynamic controller to generate required torques so as to track the desired wheel positions and velocities. Two different controllers, computed torque based proportional-integral-derivative (PID) control and sliding mode control (SMC), are introduced for the aforementioned dynamic controllers. The dynamic controllers are designed for nominal inertia parameters of the symmetric and asymmetric model dynamics based on the priori information or measurement about

the user gait parameters. Both controllers are implemented for the designed system models with time-varying inertia parameters due to the i-walker CG displacements and load changes on the i-walker. The time-varying parameters of the asymmetric model are also set with respect to the users who have symmetric and asymmetric gait patterns. The designed controllers are validated via MATLAB/Simulink, and the simulation results are presented.

Finally, instrumentation is studied to support the proposed controllers based on the developed models. For the detection of human motion intention use of a Laser range sensor and encoders is considered. Selection and mounting of sensors with adequate resolution, actuators providing required maximum torques and a processor for communication and commanding among sensors and actuators is discussed.

The thesis is organized as follows. In Chapter 2, background information is given about human-walker interaction, dynamic modelling, control and sensing, in order to well-understand the relationship between previous studies and this study. Two types of control oriented models and one high-fidelity model for the i-walker system are proposed in Chapter 3. In Chapter 4, PID control and SMC schemes are designed and combined with an inverse kinematic controller for the proposed control oriented system models. Simulation results are also given to validate the effectiveness of proposed controllers and the proposed dynamic model for the user with different gait patterns. Chapter 5 presents necessary processor, actuators, and sensors selection based on the designed controllers and system models. Finally, conclusions and future works are given in Chapter 6.

Chapter 2

Background

Independent mobility is vital for each individual to perform daily living activities without any assistance. However, human walking ability can be weakened due to age, injuries or different pathologies. This condition discourages the handicapped people from integrating into the community or using their reduced mobility capacities. Conventionally, the mentioned issues are tackled by nursing care service, which becomes insufficient to meet the increasing demands for walking aid [1]. Therefore, these handicapped people start to be isolated from society and sustain a low level quality of life. All these physiological and psychological issues for individuals with walking difficulties lead robotic researchers to develop new assistive devices which force the user to employ the residual motor capability or to restore locomotion ability via functional compensation method [2]. The main aim of the assistive devices is to improve human mobility. For this reason, various robotic assistive devices, Walking Helper [3], JARow [4], RT Walker [5], PAMM smart walker [6], have been proposed.

Over the past few decades, i-walkers have become one of the most promising assistive devices thanks to their simple structure and rehabilitation feasibility. A number of i-walkers have been developed to provide users stable and safe mobility. I-walkers are mainly classified as active and passive types according to power source yielded to the system [7]. Active type is motorized to provide more efficient motion, whereas passive type uses human power and provides only braking torque in an attempt to guide the i-walker, which makes

the passive one intrinsically safer than active one since its movement is highly dependent on the user intention [8–10]. However, passive systems increase the effort that the user has to spend for motion with i-walker, which decreases the walking efficiency. Active systems are important to deal with the efficiency issue but the safety is still a key problem due to two main reasons: the motion of the i-walker without user intention, and inexact torque generation since the load changes and CG displacement in the i-walker system due to pHWI have not been considered. This thesis proposes solutions to these problems to improve safety and efficiency for active i-walker systems. To this end, we begin with investigating the pHWI and its relationship with the user gait characteristics and dynamics. Based on this investigation, the required torques are determined for a well human-walker cooperation.

2.1 Human-Walker Interaction

The main objective of the i-walker is to partially support the user body weight for safe and stable motion. This support can reach 20% of user body weight during walking [11]. If the weight of the i-walker is assumed to be 20 kg, the applied force on the i-walker by the user, whose weight can range from 60 kg to 130 kg, highly affects the i-walker dynamics changing the total weight and the CG location of the i-walker system. The variations of the load and CG place during walking could be observed from the physical interaction of the user upper limb with the walker handles, as illustrated in Fig. 2.1. Even if the user interacts with the i-walker via upper limb, the force distribution on the i-walker shows periodic patterns similar to the user gait [12–14]. This similarity can be used to estimate the frequency of CG displacement, load changes on the i-walker and the user gait characteristics. The knowledge of these parameters could be used to achieve more realistic dynamic model and better controller for safe and efficient motion of i-walker systems. Thus, the close relation between pHWI and human gait increases the importance of the investigation of human gait for assistive and rehabilation purpose.

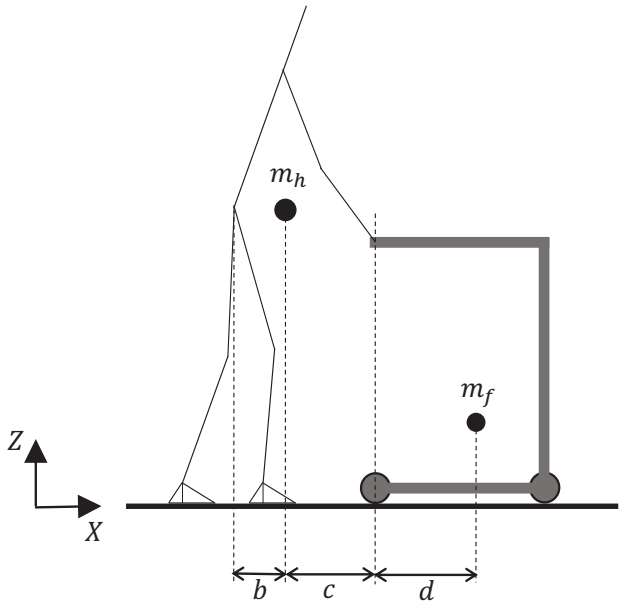

Figure 2.1: Configuration of human walker system.

2.1.1 Human Gait

Human walking is a method of locomotion involving two legs to provide support and propulsion. The term '*gait*' refers to the walking style. The '*gait cycle*' is described as the time period between two occurrences of the same event. It is possible to choose any event in gait for initiating the cycle. However, the most common start of the cycle is the instant when one heel begins contacting with the ground ('*initial contact*'). This cycle is completed with the re-contact of the same heel with the ground [15].

It is also possible to examine the gait cycle in two phases: '*stance*' and '*swing*'. The former is the phase of the gait cycle that the foot is always on the ground in order to support the body weight and provide propulsion to the body, and thus it is also called '*support*' phase. The latter is the phase that the foot is freely moving through the air [15].

The gait cycle, as depicted in Fig. 2.2, includes two periods of double support and two periods of single support. The stance and swing phases account for approximately 60%

and 40% of the gait cycle, respectively, and each period of double support lasts about 10% of the cycle, which starts from the Heel Strike of a foot and ends at the Toe Off of the opposite foot. These ratios above are highly dependent on the speed of walking [15].

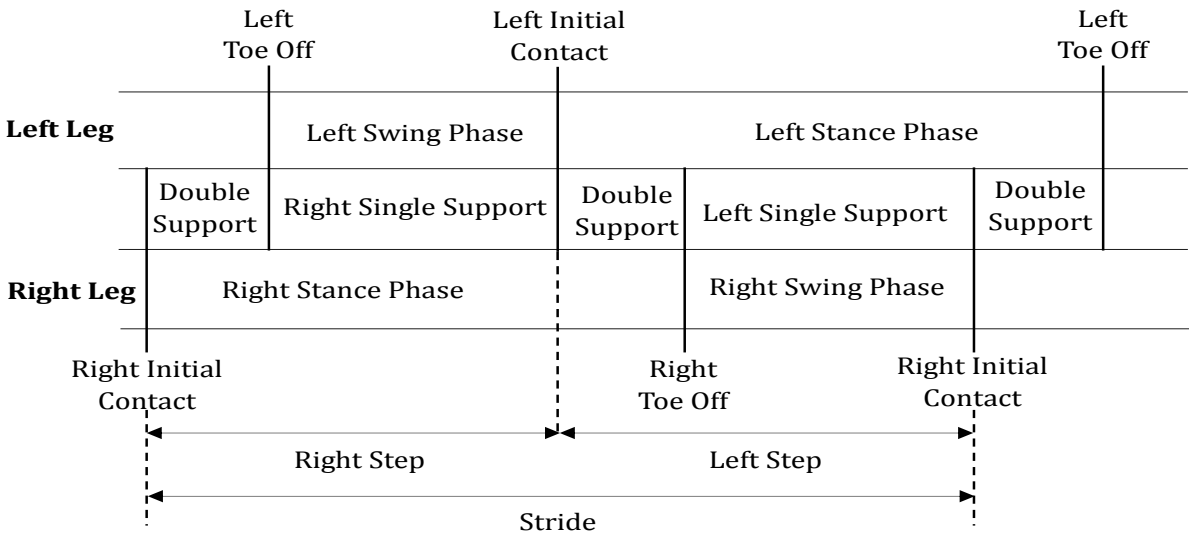

Figure 2.2: Gait timing

Other significant gait terms used in the evaluation of the user gait characteristics, *step length*, *stride length*, *cadence*, *step width*, are described as the distance between heel contacts of the opposite feet, the distance between two successive heel contacts of the same foot, and the number of steps per minute, respectively.

During walking, the CG of human body follows a path having sinusoid pattern in the sagittal (X-Z plane) and the frontal (Y-Z plane) planes. For each gait cycle human CG moves up-down twice in the sagittal plane, and left-right once in the frontal plane. In the sagittal plane, minimum CG height is at the midpoint of the double support phase (5% and 55% of the gait cycle). The CG reaches maximum height at the midpoint of single support phase (30% and 80% of the gait cycle). The CG displacement in the frontal plane also moves the maximum right and left positions at the midpoint of the single support phases. The CG displacement in the sagittal plane is dependent on the right-left step lengths and walking speed or cadence [16]. Thus, the user gait pattern directly affects the displacement

of human CG and the load on the i-walker system.

2.1.2 Human Effect on the Intelligent Walker Dynamics

I-walker physically interacts with the upper limbs of the user as seen in Fig. 2.3. This pHWI affects the dynamics of the i-walker due to the applied forces by the user on the i-walker handles. The pHWI in the sagittal plane can be described by the equations

$$\begin{aligned} F_x &= R_x - m_h \ddot{x}_h, \\ F_z &= m_h(\ddot{z}_h - g) - R_z, \\ F_z c &= R_z b \end{aligned} \tag{2.1}$$

where x_h, z_h are the location of the human CG in the X and Z axes, respectively. The human CG location is the function of the human joint angles. R_x and R_z are the total ground reaction forces in the direction of X and Z-axes. b and c are the distances between human CG and ground reaction forces, and the vertical forces on the handles in X-axis.

(2.1) implies that in addition to the user body weight and body pose, the total vertical force F_z is also dependent on the user CG motion and ground reaction forces which have periodic nature. Thus, the total load is periodically changing with the user CG motion in the sagittal plane. Moreover, each handle provides different amount of support to the user with respect to the user CG motion in the frontal plane and the user gait phase during walking. For instance, the applied vertical force on the left handle is much more than one on the right handle during single support phase of the right leg, and vice versa.

As mentioned in the previous section, the human CG displacement is closely related to the gait parameters, such as swing phase, stance phase, stride length, step width and walking speed. This implies that the user gait pattern determines the load distribution on the i-walker during walking.

In this thesis, the i-walker CG displacements and the load changes on the i-walker due to pHWI based on gait dynamics and characteristics are considered to achieve more accurate dynamic models. These dynamic models could be used in controller design of the i-walker to generate the required torques for stable i-walker human motion.

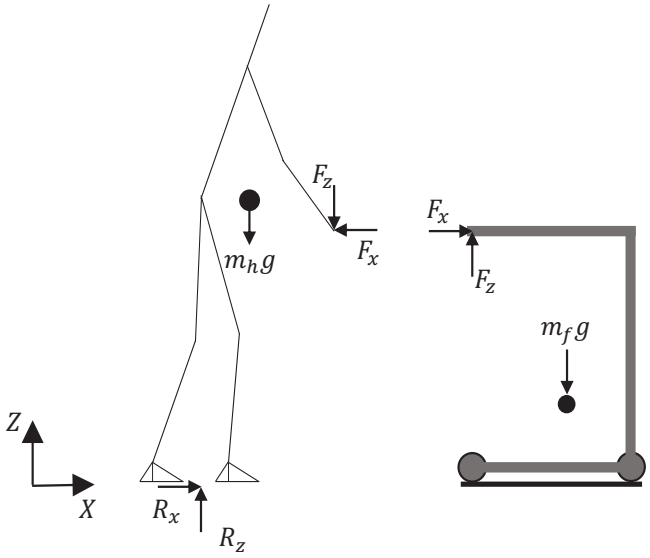

Figure 2.3: Free body diagram of human and i-walker in the saigttal plane.

2.2 Dynamic Modelling

Although there are walking aid systems having various structures [9, 10, 17–20], here we consider a standard i-walker configuration which consists of a support frame, two independently powering/braking differential wheels, one/two free caster/s, as shown in Fig. 2.4. The controllers and a sensor subsystem of the i-walker are designed considering various tasks, such as obstacle avoidance, motion guidance, human motion monitoring and rehabilitation. Since the conventional i-walker has a differential drive mechanism and a nonholonomic constraint, it shows very similar dynamic characteristic to the differential drive wheeled mobile robot (WMR).

There are two approaches to model the dynamics of the differential drive WMR: Lagrangian [22–24], and Newton-Euler [25]. Since the former has the advantage of tackling constraint forces, the Lagrangian method is more common to derive the dynamic equations. In a simple WMR dynamics [22–25] , total mass is assumed to be known and exhibit symmetric distribution over the robot. Therefore, the place of CG is assumed to be known and

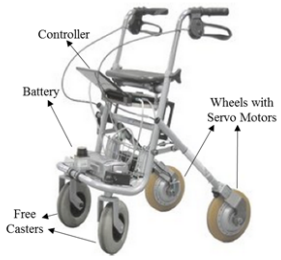

Figure 2.4: Intelligent walker [21]

fixed on the longitudinal axis of body fixed frame. There are also some studies in literature putting the CG on the axis of motorized differential wheels to simplify the dynamic of WMR. Furthermore, many research neglect the motor dynamics components like viscous damping effect, and unknown disturbances like frictions.

Though the i-walker itself has a differential drive WMR dynamics, its physical interaction with human crucially affects the i-walker dynamics. The i-walker provides support up to 20% of the user body weight [11], which means that extra inertia is added to the i-walker dynamics during walking. This extra load from human support and its applied point are periodically changing with the user CG motion which is dependent on the user gait dynamics and characteristics. Thus, the required torque for a stable and efficient motion is periodically changing during walking.

[18] considers load changes and CG shifts due to pHWI for an i-walker with mecanum wheels. [19, 26] develop a dynamic model for i-walker system having omni-directional wheels considering the CG displacement due to the weight support. However, the variations in the CG location and total load on the nonholonomic i-walker are not taken into account for a differential drive i-walker system. Moreover, none of these studies considers the gait dynamics for pHWI. This thesis proposes three dynamic models for the differential drive i-walker system. All models consider pHWI and the user gait dynamics. The dynamics of control oriented system models are designed as single-body i-walker dynamics with human effect and are categorized symmetric vs. asymmetric. We start with developing a symmetric dynamic model based on the assumption that the i-walker system CG displacements due to pHWI only occurs along the i-walker symmetry axis. Since the sym-

metric model ignore the lateral CG displacement of the i-walker system due to human CG motion in the frontal plane, an asymmetric model is proposed. The asymmetric model enables modelling and simulation for human users with different gait characteristics. The CG location parameters for both designed dynamic models are periodically changing in parallel with the user gait phases. These location changes are dependent on the vertical components of the applied forces by the user on the i-walker.

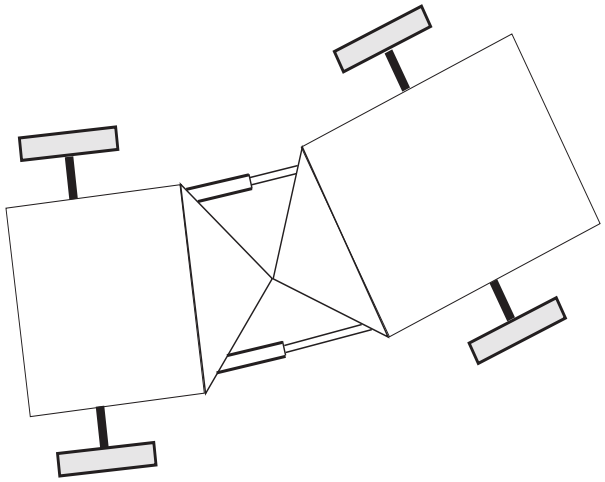

Figure 2.5: Articulated frame steering vehicles

As a third model, a high-fidelity model is developed for testing of i-walker guided human-walker systems based on multi-body dynamic approach. The model has similar dynamics to articulated frame steering vehicles' as illustrated in Fig. 2.5. This steering system is generally powered by two hydraulic actuators controlling the relative angle between two parts of the articulated vehicles. In these vehicles, the front and the rear parts are interacted with each other via inner forces at articulated joint [27]. This two-body system represents the i-walker human system in terms of interaction to each other and steering of the system. In [27, 28], for control purpose a torsional spring and damper at articulated joint are used in simplified dynamic model to represent the hydraulic cylinders between the parts of articulated steering vehicles.

2.3 Control

For assistive devices, safety and stable motion are the key properties as mentioned previously. In this regard, a considerable amount of research has been conducted on the control of assistive devices. In [7] and [10], a human adaptive motion controller is proposed for a passive nonholonomic i-walker. The designed controller adapts the dynamics of the i-walker via braking torques to the applied forces/torque by the user and environmental conditions. Thus, the maneuverability of the i-walkers are improved. [10] proposed motion control scheme based on the user states, including walking, stopped and emergency states. In [29], a human adaptive motion controller is designed for passive and active nonholonomic walking support systems. These systems are adapted to the user disabilities and states to improve the maneuverability. In [9], a robot walking helper is designed combining active and passive control modes. Passive control mode uses a braking control law. Active one is considered as gravity compensation. [14] proposes an inverse kinematic controller to move the i-walker based on the human motion intention. Two LQR controllers are proposed to compute the optimal state feedback gain for the stabilization of a two-wheeled i-walker in [17]. However, these studies do not take the dynamic effects such as CG shifts, load changes, friction, and uncertainties into consideration.

[18] proposes an adaptive based motion controller for a walking support system with mecanum wheels. The designed adaptive controller is robust to the CG shifts and load changes on the i-walker. [19, 26] also applied an adaptive control scheme for an omnidirectional wheeled walker for the CG displacement due to partial weight support. All these studies neglect the fact that the pHWI is highly dependent on the user gait dynamics. Unlike previous studies, this thesis focuses on control of an active type nonholonomic i-walker system considering the pHWI based on the user gait dynamics and characteristics.

2.4 Sensing

Sensing plays an important role to design an assistive device like the i-walker. Suitable sensor selection and their appropriate instalment could improve the safety and performance

of the i-walker system, and decrease the redundancy and cost. In the previous studies, various sensors have been used for different purposes, such as obstacle detection, the user intention and collision avoidance.

Force and pressure sensors placed on the i-walker handles are generally preferred to figure out the user motion intention and the user applied force [14, 29, 30]. In [26, 31, 32], force sensors are mounted on the armrest to understand the human directional intention. In [29], force sensor is placed between the support frame and the mobile platform. In addition to the force/torque sensors, laser range finders are also used to detect the relative location of the user with respect to the RT walker for user motion intention from user leg's distances [7, 10, 12–14]. Compared to the previous works, in this thesis, a measurement technique is presented to recognize the human motion intention from the user torso motion using a laser range finder (LRF) and magnetic encoders. Moreover, force/torque sensors are mounted on the handles to obtain user gait parameters and forces applied by the user.

Chapter 3

System Modelling

This chapter focuses on control oriented modelling of the i-walker human system. First, a general decentralized two-body kinematic model for i-walker system is derived, where the interaction between the human component and the walker component is simply described by the parameters l, ψ and ϕ in Fig. 3.1. After that, three dynamic models are developed as summarized in Fig. 3.2 ; two single-body models and one multi-body model, all taking pHWI into consideration. The two single body dynamic models focus only on the i-walker component and model the effect of vertical force components of pHWI. These models differentiate from each other in terms of CG displacement, and classified as symmetric vs. asymmetric. A high-fidelity model of the i-walker system option, the two-body dynamic model is developed based on the articulated frame steering vehicles. This two-body model considers both vertical and horizontal force components of pHWI.

3.1 Kinematic Modelling

The kinematics of human-walker motion is modelled in [34] as illustrated in Fig. 3.1. The nonholonomic i-walker is driven by two independent motors coupled with rear wheels of radius r. These wheels are separated by distance $2L$. In addition to the global reference frame, two body-fixed frames are defined. One of these body-fixed frames is placed on the

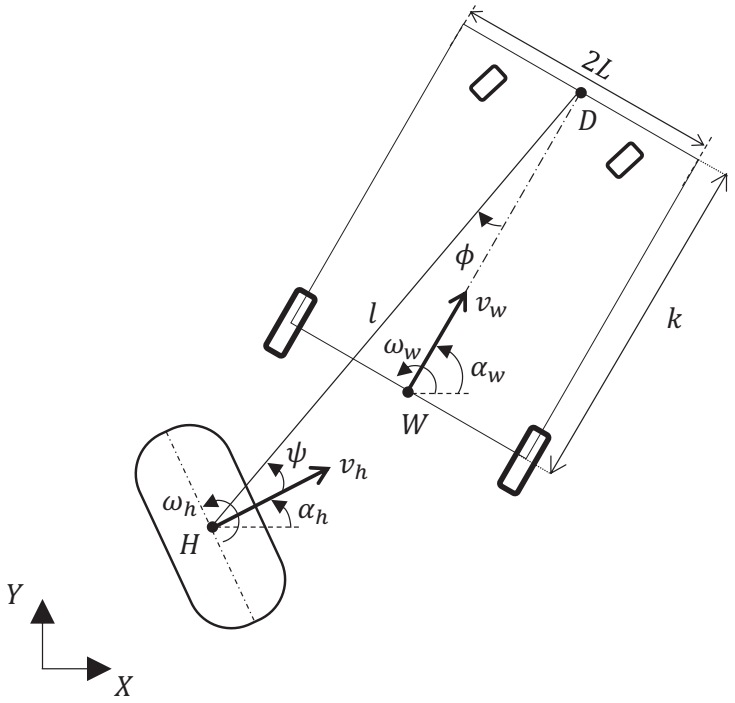

Figure 3.1: Human-walker motion kinematic model.

mid-point W on the axis between the rear wheels of the i-walker. The other one is put on the mid-point H of center of the user torso or two legs. k is the distance between the point W and the point D. There is a sensor at the point D for distance measurement.

The variables, v, ω, and α represent linear velocity, angular velocity, and orientation, respectively. The parameters for the human are described with the subscript h, whereas the walker parameters are denoted by the subscript w. Moreover, the kinematic parameters l, ψ, and ϕ of human-walker relative motion are defined as the distance between the point D and the point H, the angle between the velocity vector v_h and the line l, the angle between l and the longitudinal axis of i-walker, respectively.

The pose of the i-walker in the reference frame is specified by the vector $p_w = [x_w, y_w, \alpha_w]$ where (x_w, y_w) and α_w are the coordinates of point W and the heading angle, respectively. The kinematic equations of the i-walker are given as follows:

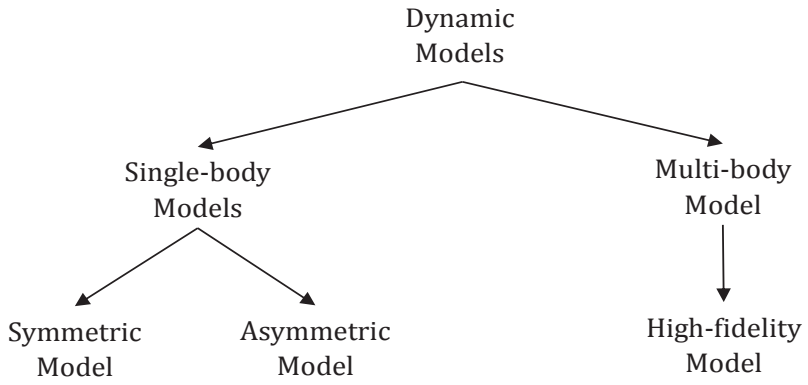

Figure 3.2: Classification of the developed i-walker system models.

$$\begin{bmatrix} \dot{x}_w \\ \dot{y}_w \\ \dot{\alpha}_w \end{bmatrix} = \begin{bmatrix} \cos\alpha_w & 0 \\ \sin\alpha_w & 0 \\ 0 & 1 \end{bmatrix} \begin{bmatrix} v_w \\ \omega_w \end{bmatrix}, \tag{3.1}$$

$$\begin{bmatrix} v_w \\ \omega_w \end{bmatrix} = \begin{bmatrix} \frac{r}{2} & \frac{r}{2} \\ \frac{r}{2L} & \frac{-r}{2L} \end{bmatrix} \begin{bmatrix} \dot{\theta}_R \\ \dot{\theta}_L \end{bmatrix} = R\dot{\eta}, \quad \eta = \begin{bmatrix} \theta_R \\ \theta_L \end{bmatrix}, \tag{3.2}$$

where R defines the kinematic relation between wheels and walker linear and angular velocities; θ_R and θ_L represent the rotational displacements of right and left powered rear wheels, respectively. The forward kinematic model of the i-walker is obtained as follows:

$$\begin{bmatrix} \dot{x}_w \\ \dot{y}_w \\ \dot{\alpha}_w \end{bmatrix} = \begin{bmatrix} r\frac{\cos\alpha_w}{2} & r\frac{\cos\alpha_w}{2} \\ r\frac{\sin\alpha_w}{2} & r\frac{\sin\alpha_w}{2} \\ \frac{r}{2L} & -\frac{r}{2L} \end{bmatrix} \begin{bmatrix} \dot{\theta}_R \\ \dot{\theta}_L \end{bmatrix} = T\dot{\eta} \tag{3.3}$$

There exist three constraint equations in the kinematic model of the i-walker, which are based on the following assumptions:

Assumption 1: There is no lateral slip, and hence the lateral velocity of the i-walker in the body-fixed frame is zero:

$$-\dot{x}_w \sin\alpha_w + \dot{y}_w \cos\alpha_w = 0. \tag{3.4}$$

Assumption 2: Each driving wheel has a pure rolling motion, i.e., the powered wheels continuously maintain their contacts with the ground, leading to the following constraint equations:

$$\begin{aligned} \dot{x}_w \cos\alpha_w + \dot{y}_w \sin\alpha_w + L\dot{\alpha}_w - r\dot{\theta}_R = 0, \\ \dot{x}_w \cos\alpha_w + \dot{y}_w \sin\alpha_w - L\dot{\alpha}_w - r\dot{\theta}_L = 0. \end{aligned} \tag{3.5}$$

Choosing $q = \begin{bmatrix} x_w & y_w & \alpha_w & \theta_R & \theta_L \end{bmatrix}^T$ as the generalized coordinate vector, the constraint equations above can be rewritten in the matrix form

$$A(q)\dot{q} = 0, \tag{3.6}$$

where the constraint matrix is

$$A(q) = \begin{bmatrix} -\sin\alpha_w & \cos\alpha_w & 0 & 0 & 0 \\ \cos\alpha_w & \sin\alpha_w & L & -r & 0 \\ \cos\alpha_w & \sin\alpha_w & -L & 0 & -r \end{bmatrix}.$$

The forward kinematic equations of the point W are obtained as

$$\dot{q} = S(q)\dot{\eta}, \tag{3.7}$$

where

$$S(q) = \begin{bmatrix} \frac{r}{2}\cos\alpha_w & \frac{r}{2}\cos\alpha_w \\ \frac{r}{2}\sin\alpha_w & \frac{r}{2}\sin\alpha_w \\ \frac{r}{2L} & -\frac{r}{2L} \\ 1 & 0 \\ 0 & 1 \end{bmatrix}$$

The time derivative of (3.7) is given as

$$\ddot{q} = \dot{S}(q)\dot{\eta} + S(q)\ddot{\eta}. \tag{3.8}$$

Assuming that a full rank matrix $S(q)$ is formed by a set of smooth and linearly independent vector fields spanning the null space of $A(q)$, which satisfies the equation

$$S^T(q)A^T(q) = 0. \tag{3.9}$$

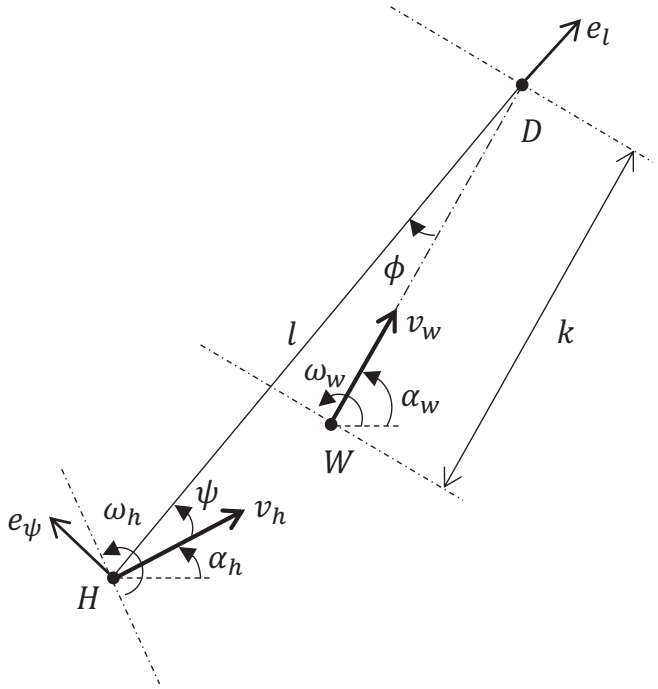

Figure 3.3: Human-walker motion kinematic model in polar coordinates.

The kinematic equations of the i-walker human relative motion, as seen in Fig. 3.1, are derived using polar coordinates. To this end, the local frame is placed on the point H, and the coordinates are defined as e_ψ and e_l, as illustrated in Fig. 3.3. We assume that the parameters, v_h, ω_h, v_w, ω_w, l and ψ are continuously obtained by suitable sensors and measurement techniques. Then, we can use the velocity equalities of common point D to derive the kinematic equations

$$\begin{aligned} l(\omega_h + \dot{\phi}) - v_h \sin\psi &= k\omega_w \cos\phi + v_w \sin\phi, \\ v_h \cos(\psi) + \dot{l} &= v_w \cos\phi - kw_w \sin\phi. \end{aligned} \tag{3.10}$$

The kinematic model of the human-walker relative motion is defined as follows:

$$\begin{bmatrix} \dot{l} \\ \dot{\psi} \end{bmatrix} = \begin{bmatrix} \cos\phi & -k\sin\phi \\ \frac{\sin\phi}{l} & k\frac{\cos\phi}{l} \end{bmatrix} \begin{bmatrix} v_w \\ \omega_w \end{bmatrix} + \begin{bmatrix} -v_h\cos\psi \\ -\omega_h + v_h\frac{\sin\psi}{l} \end{bmatrix} \tag{3.11}$$

The inverse kinematic model of (3.11) is given

$$\begin{bmatrix} v_w \\ \omega_w \end{bmatrix} = \begin{bmatrix} \cos\phi & l\sin\phi \\ -\frac{\sin\phi}{k} & l\frac{\cos\phi}{k} \end{bmatrix} \begin{bmatrix} \dot{l} + v_h\cos\psi \\ \dot{\psi} + \omega_h - v_h\frac{\sin\psi}{l} \end{bmatrix}, \tag{3.12}$$

where $\phi = \alpha_w - \alpha_h - \psi$.

3.2 Single-body Models

In this section, two single-body models are designed based on the pHWI related to gait dynamics. The models are classified as symmetric and asymmetric. Symmetric one is designed for the CG displacement on the symmetric axis (x). Then, the asymmetric model is developed considering the CG displacements both in lateral (y) and symmetric axes during walking. Based on these descriptions, their dynamic models are defined.

3.2.1 Symmetric Model

For the symmetric model as shown in Fig. 3.4, motor viscous damping effects and torque disturbances from unknown frictions are added to the system. The distance, d, of CG from the point W depends on the user weight and body pose during walking. The parameter d is periodically changing with respect to the user gait cycle. The main assumption for this model is that the CG location only changes along with the longitudinal axis of the i-walker.

The Lagrange formalism is very common to derive the dynamic equation of non-holonomic differential wheeled mobile platforms to eliminate the constraint forces.

$$\frac{d}{dt}\left(\frac{\partial L}{\partial \dot{q}_i}\right) - \frac{\partial L}{\partial q_i} = F - A^T(q)\lambda, \tag{3.13}$$

where L is the Lagrangian function, which is the difference between kinetic and potential energy of the whole system. F is generalized force vector, and λ is the vector of the

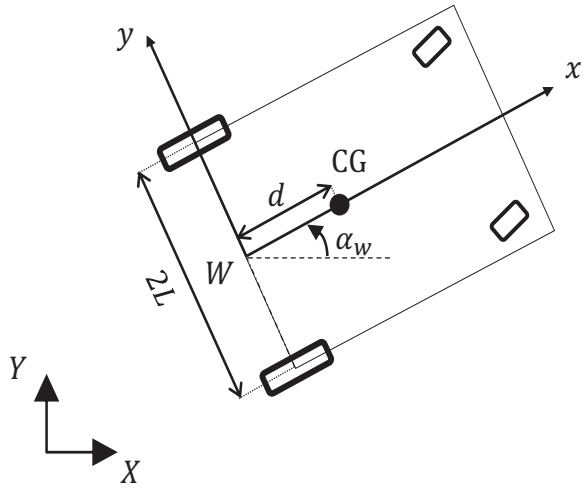

Figure 3.4: Symmetric dynamic model of i-walker.

Lagrange multipliers. The kinetic energy of the system consists of the kinetic energies of wheels with actuators and support frame with human effect.

$$\begin{aligned} T_c &= \frac{1}{2} m_c v_c^2 + \frac{1}{2} I_c \dot{\alpha}_w^2, \\ T_{wR} &= \frac{1}{2} m_w v_{w_R}^2 + \frac{1}{2} I_m \dot{\alpha}_w^2 + \frac{1}{2} I_w \dot{\theta}_R^2, \\ T_{wL} &= \frac{1}{2} m_w v_{w_L}^2 + \frac{1}{2} I_m \dot{\alpha}_w^2 + \frac{1}{2} I_w \dot{\theta}_L^2, \end{aligned} \tag{3.14}$$

where T_c represents the kinetic energy of the frame with the user partial support, T_{wR} and T_{wL} are the kinetic energies of each wheel including actuators. m_c represents the mass of the support frame with human effect. m_w is the mass of each driven wheel with a motor. I_c is the moment of inertia of the support frame about the vertical axis through the CG, I_w and I_m are the moment of inertia of each powered wheel with a motor about the wheel axis and the wheel diameter, respectively. v_{wR} and v_{wL} are the linear velocities of the powered wheels. The total kinetic energy of the system based on (3.14) is

$$T = \frac{1}{2}m\left(\dot{x}_w^2 + \dot{y}_w^2\right) + m_c d\dot{\alpha}_w\left(\dot{y}_w cos\alpha - \dot{x}_w sin\alpha\right) + \frac{1}{2}I_w\left(\dot{\theta}_R^2 + \dot{\theta}_L^2\right) + \frac{1}{2}I\dot{\alpha}_w^2, \tag{3.15}$$

where $m = m_c + 2m_w$ and $I = I_c + m_c d^2 + 2m_w L^2 + 2I_m$. Since the system is moved in plane, the potential energy does not change, and can be considered as zero putting the reference at suitable height. Substituting (3.15) in (3.13), the dynamic model of the i-walker is obtained as follows:

$$M(q)\ddot{q} + C(q,\dot{q})\dot{q} = B(q)\tau - A^T(q)\lambda, \tag{3.16}$$

where $M(q)$, $C(q,\dot{q})$, $B(q)$, and τ are the symmetric positive definite inertia matrix, the centripetal and Coriolis matrix, the input matrix, and the torque vector, respectively, whose detailed forms are as follows:

$$M(q) = \begin{bmatrix} m & 0 & -m_c d\sin\alpha_w & 0 & 0 \\ 0 & m & m_c d\cos\alpha_w & 0 & 0 \\ -m_c d\sin\alpha_w & m_c d\cos\alpha_w & I & 0 & 0 \\ 0 & 0 & 0 & I_w & 0 \\ 0 & 0 & 0 & 0 & I_w \end{bmatrix},$$

$$C(q,\dot{q}) = \begin{bmatrix} 0 & 0 & -m_c d\dot{\alpha}_w\cos\alpha_w & 0 & 0 \\ 0 & 0 & -m_c d\dot{\alpha}_w\sin\alpha_w & 0 & 0 \\ 0 & 0 & 0 & 0 & 0 \\ 0 & 0 & 0 & b_m & 0 \\ 0 & 0 & 0 & 0 & b_m \end{bmatrix}, \quad B(q) = \begin{bmatrix} 0 & 0 \\ 0 & 0 \\ 0 & 0 \\ 1 & 0 \\ 0 & 1 \end{bmatrix}, \quad \tau = \begin{bmatrix} \tau_R \\ \tau_L \end{bmatrix},$$

where b_m is the viscous damping on the motor. (3.16) can be put into a more appropriate form of (3.16) for simulation and control purposes by eliminating the constraint term $A^T(q)\lambda$ [35].

Substituting (3.7) and (3.8) into (3.16), and then multiplying both sides from left by $S^T(q)$, the reduced dynamic model is obtained in the following form

$$\bar{M}\ddot{\eta} + \bar{C}\dot{\eta} = \bar{B}\tau, \tag{3.17}$$

where

$$\begin{aligned}\bar{M} &= S^T(q)M(q)S(q)\\ \bar{C} &= S^T(q)M(q)\dot{S}(q) + S^T(q)C(q,\dot{q})S(q),\\ \bar{B} &= S^T(q)B(q).\end{aligned} \tag{3.18}$$

Open forms of the $\bar{M}$, $\bar{C}$, $\bar{B}$, and τ are as follows:

$$\bar{M} = \begin{bmatrix} \frac{mr^2}{4} + \frac{Ir^2}{4L^2} + I_w & \frac{mr^2}{4} - \frac{Ir^2}{4L^2} \\ \frac{mr^2}{4} - \frac{Ir^2}{4L^2} & \frac{mr^2}{4} + \frac{Ir^2}{4L^2} + I_w \end{bmatrix}, \quad \tau = \begin{bmatrix} \tau_R \\ \tau_L \end{bmatrix},$$

$$\bar{C} = \begin{bmatrix} b_m & \frac{m_c r^2 d}{2L}\dot{\alpha}_w \\ -\frac{m_c r^2 d}{2L}\dot{\alpha}_w & b_m \end{bmatrix}, \quad \bar{B} = \begin{bmatrix} 1 & 0 \\ 0 & 1 \end{bmatrix}.$$

3.2.2 Asymmetric Model

The asymmetric model is developed to include the lateral CG displacement of the i-walker in dynamic modelling. The main idea is that the user gait phase and the sinusoidal motion of the user CG in the frontal plane cause the asymmetric load on the i-walker. In other words, the amount of applied force on each handle is not equal to each other during gait cycle. The magnitude and variations of the forces on the handles are dependent on the user weight, pose, gait dynamics and gait characteristics. The developed asymmetric model is illustrated in Fig. 3.5.

The only difference from the symmetric model is allowing the angle β which is defined as the angle between longitudinal axis and the position vector d. The parameters, d, β, are dependent on the user weight, body pose and gait pattern (e.g., asymmetric or symmetric). The location of CG is redefined as follows:

$$\begin{aligned} x_C &= x_w + d\cos(\alpha_w + \beta),\\ y_C &= y_w + d\sin(\alpha_w + \beta). \end{aligned} \tag{3.19}$$

The velocities of CG in the global frame becomes

$$\begin{aligned} \dot{x}_C &= \dot{x}_w - d\dot{\alpha}_w\sin(\alpha_w + \beta),\\ \dot{y}_C &= \dot{y}_w + d\dot{\alpha}_w\cos(\alpha_w + \beta). \end{aligned} \tag{3.20}$$

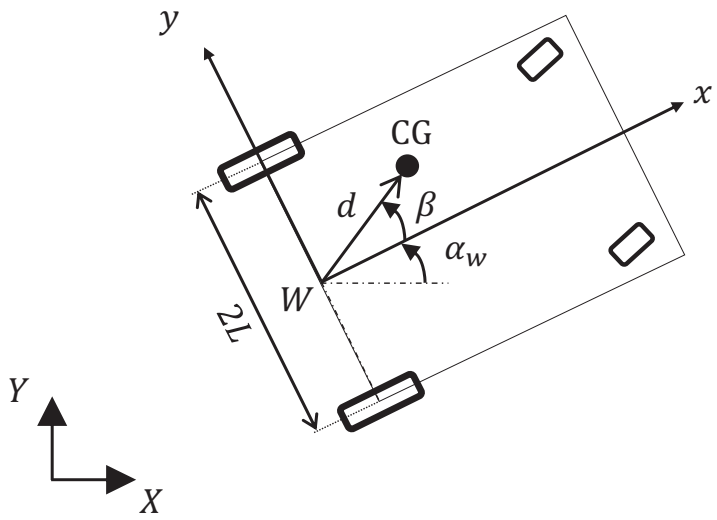

Figure 3.5: Asymmetric model of i-walker.

The square of longitudinal velocity of the i-walker system CG is

$$v_c^2 = \dot{x}_w^2 + \dot{y}_w^2 + d^2\dot{\alpha}_w^2 + 2d\dot{\alpha}_w[\dot{y}_w\cos(\alpha_w+\beta) - \dot{x}_w\sin(\alpha_w+\beta)]. \tag{3.21}$$

Substituting (3.21) in (3.14), the kinetic energy of walker with human effect is computed, and then the total kinetic energy of the i-walker system, (3.15) is derived as

$$T = \frac{1}{2}m\left(\dot{x}_w^2+\dot{y}_w^2\right) + m_c d\dot{\alpha}_w\left[\dot{y}_w\cos(\alpha_w+\beta) - \dot{x}_w\sin(\alpha_w+\beta)\right] + \frac{1}{2}I_w\left(\dot{\theta}_R^2+\dot{\theta}_L^2\right) + \frac{1}{2}I\dot{\alpha}_w^2 \tag{3.22}$$

The potential energy is considered as zero due to the planar motion of the system. Applying Lagrange Formula in (3.13), M and C matrices for the asymmetric model are obtained as follows:

$$M(q) = \begin{bmatrix} m & 0 & -m_c d\sin(\alpha_w+\beta) & 0 & 0 \\ 0 & m & m_c d\cos(\alpha_w+\beta) & 0 & 0 \\ -m_c d\sin(\alpha_w+\beta) & m_c d\cos(\alpha_w+\beta) & I & 0 & 0 \\ 0 & 0 & 0 & I_w & 0 \\ 0 & 0 & 0 & 0 & I_w \end{bmatrix},$$

$$C(q,\dot{q}) = \begin{bmatrix} 0 & 0 & -m_c d\dot{\alpha}_w\cos(\alpha_w+\beta) & 0 & 0 \\ 0 & 0 & -m_c d\dot{\alpha}_w\sin(\alpha_w+\beta) & 0 & 0 \\ 0 & 0 & 0 & 0 & 0 \\ 0 & 0 & 0 & b_m & 0 \\ 0 & 0 & 0 & 0 & b_m \end{bmatrix}$$

The reduced order matrices are obtained applying (3.18):

$$\bar{M} = \begin{bmatrix} -\frac{m_c d r^2\sin\beta}{2L} + \frac{mr^2}{4} + \frac{Ir^2}{4L^2} + I_w & \frac{mr^2}{4} - \frac{Ir^2}{4L^2} \\ \frac{mr^2}{4} - \frac{Ir^2}{4L^2} & \frac{m_c d r^2\sin\beta}{2L} + \frac{mr^2}{4} + \frac{Ir^2}{4L^2} + I_w \end{bmatrix}, \quad \tau = \begin{bmatrix} \tau_R \\ \tau_L \end{bmatrix},$$

$$\bar{C} = \begin{bmatrix} b_m & \frac{m_c r^2 d\cos\beta}{2L}\dot{\alpha}_w \\ -\frac{m_c r^2 d\cos\beta}{2L}\dot{\alpha}_w & b_m \end{bmatrix}, \quad \bar{B} = \begin{bmatrix} 1 & 0 \\ 0 & 1 \end{bmatrix}.$$

3.3 Multi-body Model

In this section, a high-fidelity model is proposed to investigate the effects of the horizontal and vertical force components of pHWI on the i-walker system dynamics. The model is designed based on multi-body approach resembling the articulated frame steering vehicles. There are two bodies in the model, one of which represents the i-walker and the other refers to the user. The user is considered as a unicycle wheeled mobile platform embedded to the i-walker. The CG location of the unicycle wheeled platform is periodically changing along with the lateral and vertical axes in the user local frame during motion. This CG motion represents the human CG displacement in frontal and sagittal plane during walking. The

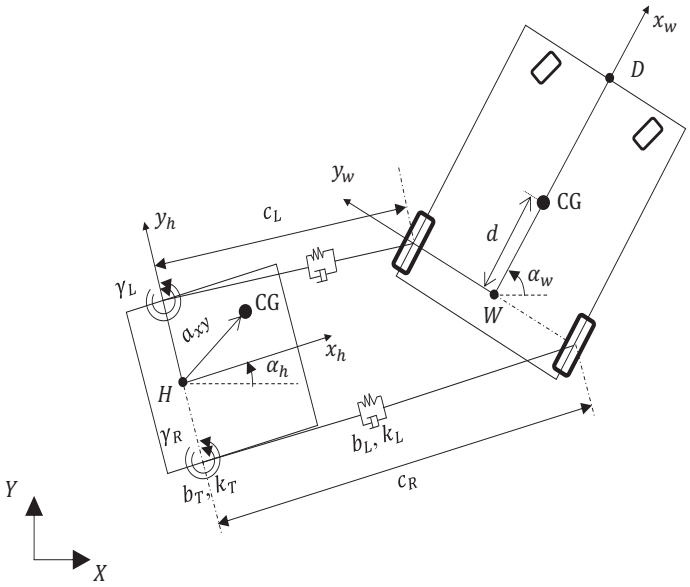

Figure 3.6: The representation of the i-walker human system as two-body wheeled mobile platform.

applied steering forces by the user are resembled by springs and dampers. For representing rotational forces applied by each human shoulder and wrist, torsional springs and dampers are used. The applied pull-push forces through human upper limbs are described as linear springs and dampers. The coefficients of all these springs and dampers are determined by the characteristic of the pHWI.

3.3.1 High-fidelity Model

The body diagram given in Fig. 3.6 is highly nonlinear and complicated for modelling purposes. To simplify this body diagram, as illustrated in Fig. 3.7, the following assumptions can be made at lower speed motion:

1) The linear spring and damping effects on the upper limbs are ignored.

2) The center of rotation point for human is fixed at the point W during motion.

3) The i-walker human motion is guided by the i-walker.

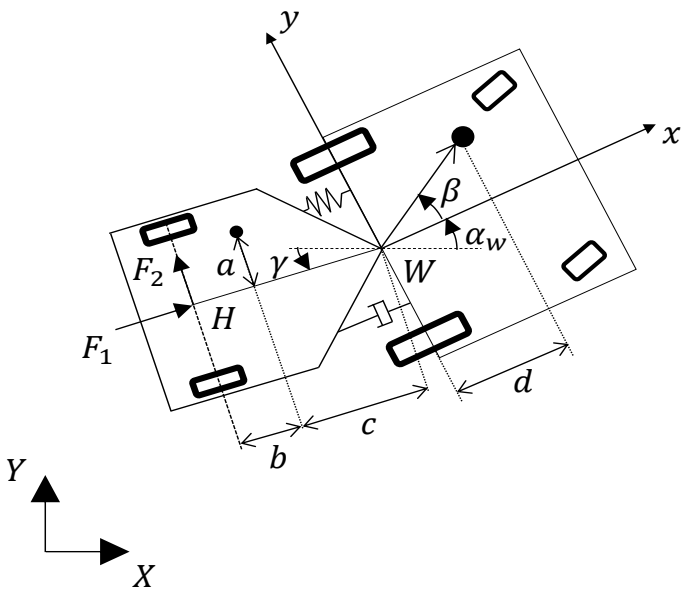

Figure 3.7: The proposed high-fidelity model.

To model the two-body dynamics, we start with the redefinition of the system kinematics. Unlike the single body models which have 2 DOF, the two-body model has 3 DOF. Thus, the generalized coordinates is augmented to $q = \begin{bmatrix} x_w & y_w & \alpha_w & \gamma & \theta_R & \theta_L \end{bmatrix}^T$. The constraint equations, (3.4), (3.5) are also valid for the high-fidelity model and written in the matrix form

$$A(q)\dot{q} = \begin{bmatrix} -\sin\alpha_w & \cos\alpha_w & 0 & 0 & 0 & 0 \\ \cos\alpha_w & \sin\alpha_w & L & 0 & -r & 0 \\ \cos\alpha_w & \sin\alpha_w & -L & 0 & 0 & -r \end{bmatrix} \begin{bmatrix} \dot{x_w} \\ \dot{y_w} \\ \dot{\alpha}_w \\ \dot{\gamma} \\ \dot{\theta}_R \\ \dot{\theta}_L \end{bmatrix}.$$

The forward kinematic equations for the system motion is in the matrix form

$$\dot{q} = S(q)\dot{z} = \begin{bmatrix} \dot{x}_w \\ \dot{y}_w \\ \dot{\alpha}_w \\ \dot{\gamma} \\ \dot{\theta}_R \\ \dot{\theta}_L \end{bmatrix} = \begin{bmatrix} 0 & \frac{r}{2}cos\alpha_w & \frac{r}{2}cos\alpha_w \\ 0 & \frac{r}{2}sin\alpha_w & \frac{r}{2}sin\alpha_w \\ 0 & -\frac{r}{2L} & \frac{r}{2L} \\ 1 & 0 & 0 \\ 0 & 1 & 0 \\ 0 & 0 & 1 \end{bmatrix} \begin{bmatrix} \dot{\gamma} \\ \dot{\theta}_R \\ \dot{\theta}_L \end{bmatrix}, \tag{3.23}$$

where $S(q)$ is a full rank matrix and the null space of $A(q)$.

The dynamic equation of the system can be derived via the Lagrange approach. The formula (3.13) can be modified adding dissipative function R

$$\frac{d}{dt}\left(\frac{\partial L}{\partial \dot{q}_i}\right) - \frac{\partial L}{\partial q_i} + \frac{\partial R}{\partial \dot{q}_i} = F - A^T(q)\lambda, \tag{3.24}$$

The kinetic energy of the i-walker with human effect for asymmetric model has already been obtained in (3.22). The user kinetic energy can be formulated as:

$$T_h = \frac{1}{2}m_h v_{hc}^2 + \frac{1}{2}I_h\dot{\gamma}^2, \tag{3.25}$$

where m_h is the mass of difference between human mass and supported mass by the i-walker. I_h, v_{hc} are the moment of inertia for human and the velocity of human CG, respectively. The location of human CG with respect to the point W is defined by the following kinematic relations:

$$\begin{aligned} x_{hc} &= x_w - c\cos\gamma - a\sin\gamma, \\ y_{hc} &= y_w - c\sin\gamma - a\cos\gamma. \end{aligned} \tag{3.26}$$

The square of human CG velocity for deriving the kinetic energy is found as

$$v_{hc}^2 = \dot{x}_w^2+\dot{y}_w^2+\dot{\gamma}^2(c^2+a^2)+2c\dot{\gamma}(\dot{x}_w\sin\gamma-\dot{y}_w\cos\gamma)+2a\dot{\gamma}(\dot{y}_w\sin\gamma-\dot{x}_w\cos\gamma)-4ac\dot{\gamma}^2\sin\gamma\cos\gamma \tag{3.27}$$

The total kinetic energy for the two-body dynamic model is derived as

$$\begin{aligned} T = \frac{1}{2}m_T\left(\dot{x}_w^2+\dot{y}_w^2\right) + m_c d\dot{\alpha}_w\left(\dot{y}_w\cos(\alpha_w+\beta) - \dot{x}_w\sin(\alpha_w+\beta)\right) + m_h c\dot{\gamma}\left(\dot{x}_w\cos\gamma - \dot{y}_w\sin\gamma\right) \\ +m_h a\dot{\gamma}\left(\dot{y}_w\sin\gamma - \dot{x}_w\cos\gamma\right) - 2m_h ac\dot{\gamma}^2\sin\gamma\cos\gamma + \frac{1}{2}I_w\left(\dot{\theta}_R^2+\dot{\theta}_L^2\right) + \frac{1}{2}I\dot{\alpha}^2 + \frac{1}{2}I_{hw}\dot{\gamma}^2, \end{aligned} \tag{3.28}$$

where $m_T = m_h + m_c + 2m_w$ and $I_{hw} = I_h(a^2 + c^2)m_h$. T is the total kinetic energy of partially supported human mass and the i-walker with human effect (3.22). The potential energy of the i-walker human system, V is

$$V = \frac{1}{2}k_R(\alpha_w - \gamma)^2, \tag{3.29}$$

where k_R is the coefficient of the torsional spring at the point W. The dissipation function of the system R is computed as

$$R = \frac{1}{2}b_R(\dot{\alpha}_w - \dot{\gamma})^2, \tag{3.30}$$

where b_R is the coefficient of the torsional damper at the articulation point W. The resultant dynamic model will be held in the following form

$$M(q)\ddot{q} + C(q,\dot{q})\dot{q} + R(\dot{q}) + V(q) = B(q)Q - A^T(q)\lambda, \tag{3.31}$$

where $R(\dot{q})$, $V(q)$ and Q are the dissipative force vector, conservative force vector and generalized force vector, respectively. The generalized force vector is $Q = \begin{bmatrix} F_1 & F_2 & 0 & 0 & \tau_R & \tau_L \end{bmatrix}^T$ .The entries of matrices, M,C, and the other matrices and vectors are given in the Appendix.

Chapter 4

Controller Design for Different Models

The main aim of control design in this chapter is to generate the required control torques, τ_R and τ_L, to keep the i-walker in front of the user such that the angle $\psi \to 0$ and the distance, $l \to l_d$ as $t \to \infty$ in Fig. 3.1, where l_d is desired human distance from the point D on the i-walker. In this regard, an inverse kinematic controller in [34] is implemented to obtain the desired linear and angular velocities of the i-walker, v_{wd}, ω_{wd}, based on the human motion and orientation. These desired velocities are transformed into the desired wheel angular velocities, $\dot{\eta}_d = \begin{bmatrix} \dot{\theta}_{Rd} & \dot{\theta}_{Ld} \end{bmatrix}^T$, using (3.2). Then, the dynamic controller is designed to generate appropriate motor torques in order to track the desired wheel positions and velocities. To this end, two types of control schemes, PID controller and sliding mode controller (SMC) are separately implemented as a dynamic controller. Then, these dynamic controllers are combined with feedback linearization unit based on computed torque control law. The block diagram of overall control design is shown in Fig. 4.1.

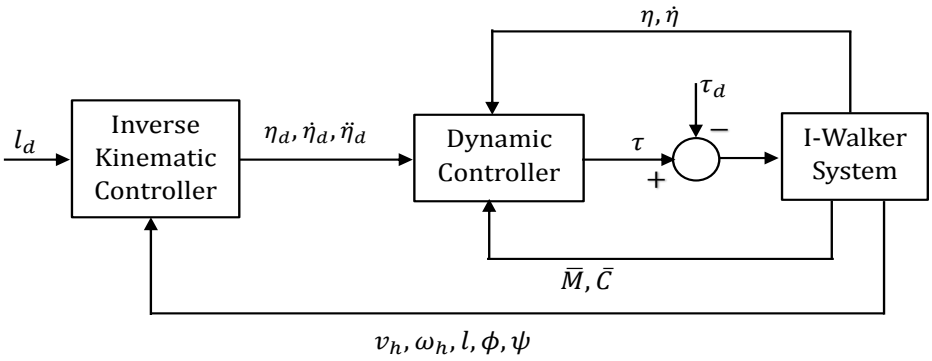

Figure 4.1: Control design of i-walker system.

4.1 Inverse Kinematic Controller Based on Human Intention

The inverse kinematic control scheme for the given model in Fig. 3.1 is proposed in [34] to control the angle ψ and the distance l. The designed controller aims at maintaining desired human-walker distance and making ψ exponentially converged to zero, which keeps the i-walker in front of human according to human relative position and orientation during walking. In other words, human intention is detected based on human kinematic data, and thus the desired i-walker angular and linear velocities are produced. The kinematic model (3.11) for our control purpose is rewritten as

$$\begin{bmatrix} \dot{\tilde{l}} \\ \dot{\psi} \end{bmatrix} = \begin{bmatrix} \cos\phi & -k\sin\phi \\ \frac{\sin\phi}{l} & k\frac{\cos\phi}{l} \end{bmatrix} \begin{bmatrix} v_w \\ \omega_w \end{bmatrix} + \begin{bmatrix} -v_h\cos\psi \\ -\omega_h + v_h\frac{\sin\psi}{l} \end{bmatrix}, \tag{4.1}$$

where $\tilde{l} = l - l_d$. The inverse kinematic control scheme is obtained using the inverse kinematic of human-walker motion in (3.12).

$$\begin{bmatrix} v_w \\ \omega_w \end{bmatrix} = \begin{bmatrix} \cos\phi & l\sin\phi \\ -\frac{\sin\phi}{k} & l\frac{\cos\phi}{k} \end{bmatrix} \begin{bmatrix} -k_l\tilde{l} + v_h\cos\psi \\ -k_\psi\psi + \omega_h - v_h\frac{\sin\psi}{l} \end{bmatrix}, \tag{4.2}$$

where k_l, k_ϕ are positive control gains.

For realization of the human-walker system, the length l, the angles ϕ and ψ, and the velocities v_w, w_w, v_h and w_h, can be obtained using a suitable sensor system and estimation method. After obtaining virtual velocity control inputs in terms of desired wheel velocities, feedback linearization technique is implemented to compute the required torques.

4.2 Feedback Linearization

In this section, feedback linearization technique is applied for tracking problem based on *the computed torque control* approach [36]. The main idea of feedback linearization is to express the nonlinear system as an equivalent linear system. The system dynamics in (3.17) is redefined considering the torque disturbance τ_d due to the unknown frictions:

$$\bar{M}\ddot{\eta} + \bar{C}\dot{\eta} + \tau_d = \tau. \tag{4.3}$$

A desired trajectory is selected as $\eta_d = [\theta_{Rd} \quad \theta_{Ld}]^T$, then tracking error is defined as follows:

$$e = \eta_d - \eta \tag{4.4}$$

Integration and derivatives of the tracking error for PID controller can be expressed as

$$\begin{aligned} \dot{e} &= \dot{\eta}_d - \dot{\eta}, \\ \ddot{e} &= \ddot{\eta}_d - \ddot{\eta}. \end{aligned} \tag{4.5}$$

Substituting (4.5) in (4.3), the following equation is obtained:

$$\ddot{e} = \ddot{\eta}_d + \bar{M}^{-1}(\bar{C}\dot{\eta} - \tau + \tau_d). \tag{4.6}$$

The control input function and the disturbance functions are defined as

$$\begin{aligned} u &= \ddot{\eta}_d + \bar{M}^{-1}(\bar{C}\dot{\eta} - \tau), \\ \omega &= \bar{M}^{-1}\tau_d. \end{aligned} \tag{4.7}$$

Defining a state as $E \in \mathbb{R}^4$, $E = \begin{bmatrix} e \\ \dot{e} \end{bmatrix}$, tracking error dynamics are written in the form

$$\dot{E} = \begin{bmatrix} 0 & I \\ 0 & 0 \end{bmatrix} E + \begin{bmatrix} 0 \\ I \end{bmatrix} u + \begin{bmatrix} 0 \\ I \end{bmatrix} \omega \tag{4.8}$$

With the feedback linearization transform (4.7), *the computed torque control law* is written as follows:

$$\tau = \bar{M}(\ddot{\eta}_d - u) + \bar{C}\dot{\eta}. \tag{4.9}$$

4.3 PID Controller

The non-linear computed torque control input allows to choose $u(t)$ as a linear control signal which makes the tracking error system (4.8) stable so that $e(t)$ goes to zero with time [36]. In this section, $u(t)$ is picked as PID feedback control input.

$$\begin{aligned} u &= -K_v\dot{e} - K_p e - K_i\varepsilon \\ \dot{\varepsilon} &= e \end{aligned} \tag{4.10}$$

Substituting (4.10) in (4.9), the computed torque control law is expressed as follows:

$$\tau = \bar{M}(\ddot{\eta}_d + K_v\dot{e} + K_p e + K_i\varepsilon) + \bar{C}\dot{\eta}. \tag{4.11}$$

The closed-loop system is given in the following state-space form

$$\begin{bmatrix} \dot{\varepsilon} \\ \dot{e} \\ \ddot{e} \end{bmatrix} = \underbrace{\begin{bmatrix} 0 & I & 0 \\ 0 & 0 & I \\ -K_i & -K_p & -K_v \end{bmatrix}}_{K} \begin{bmatrix} \varepsilon \\ e \\ \dot{e} \end{bmatrix} + \begin{bmatrix} 0 \\ 0 \\ I \end{bmatrix} \omega \tag{4.12}$$

The closed-loop characteristic polynomial is

$$\Delta_c(s) = |s^3 I + K_v s^2 + K_p s + K_i|, \tag{4.13}$$

where $K_v = diag(k_{v_i})$, $K_p = diag(k_{p_i})$, and $K_i = diag(k_{i_i})$ are the control gains [36]. We can find the following equation utilizing these gains:

$$\Delta_c(s) = \prod_{i=1}^{n}(s^3 I + k_{v_i} s^2 + k_{p_i} s + k_{i_i}). \tag{4.14}$$

For the closed-loop stability, the Routh criteria is satisfied when

$$k_{v_i} k_{p_i} > k_{i_i}. \tag{4.15}$$

4.4 Sliding Mode Control

Sliding mode control is a well known robust controller design technique in the systems with uncertainty and disturbance [38]. It consists of two important sections. First section is the design of a sliding surface to provide the tracking error goes to zero. Second section is the selection of a control law to apply the sliding surface. An integral control is also augmented to deal with constant torque disturbance in the system. Consider the general formula of the system given in (4.3).

Defining $X = \begin{bmatrix} \eta \\ \dot{\eta} \end{bmatrix}$, we can obtain the following equation

$$\ddot{\eta} = -\bar{M}^{-1}\bar{C}\dot{\eta} + \bar{M}^{-1}\tau \tag{4.16}$$

(4.16) can be rewritten as follows:

$$\ddot{\eta} = f(X) + g(X)\tau, \tag{4.17}$$

where

$$f(X) = -\bar{M}^{-1}(X)\,\bar{C}(X)\,\dot{\eta}, \tag{4.18}$$

$$g(X) = \bar{M}^{-1}(X). \tag{4.19}$$

Tracking error is redefined as

$$\bar{E} = \begin{bmatrix} \varepsilon^T & e^T & \dot{e}^T \end{bmatrix}^T = \begin{bmatrix} \varepsilon^T & E^T \end{bmatrix}^T \tag{4.20}$$

Sliding surface guarantees that the tracking error goes to zero in finite time. A time varying sliding surface can be defined in the following form

$$s(\bar{E}, t) = \dot{e} + 2\lambda e + \lambda^2 \varepsilon, \quad \lambda > 0, \tag{4.21}$$

where λ is a positive constant. SMC is designed to move (4.21) to zero. Lyapunov function can be written as

$$V_s = \frac{s^T s}{2} \tag{4.22}$$

and its derivative is written in the following form

$$\dot{V}_s = s^T \dot{s} = -k_1 \parallel s \parallel, \quad k_1 > 0, \tag{4.23}$$

where k_1 is some design constant. This condition will guarantee that the sliding surface is achieved in finite time. Control law can be selected so that the derivative of s satisfies

$$\dot{s} = -k_1 sgn(s), \tag{4.24}$$

where

$$sgn(s) = sgn\left(\left[s_1, s_2\right]^T\right) = \left[sgn(s_1), sgn(s_2)\right]^T \tag{4.25}$$

To satisfy (4.24), the control input τ is designed. First, τ_0 is selected as

$$\tau_0 = g^{-1}(X)\left(f(X) - \ddot{\eta}_d - \lambda \dot{e}\right) \tag{4.26}$$

then, the control input τ can be selected as:

$$\tau = \tau_0 - g^{-1}(X) k_1 sgn(s) \tag{4.27}$$

4.5 Simulations

In this section, the proposed controllers are implemented to the symmetric and asymmetric i-walker models in the MATLAB/Simulink environment. The physical parameters of the i-walker are given as $r = 0.15\ m$, $L = 0.27\ m$, $k = 0.65\ m$, $b_m = 0.4\ kg.m^2/s$, $I_c = 5.2\ kg.m^2$,

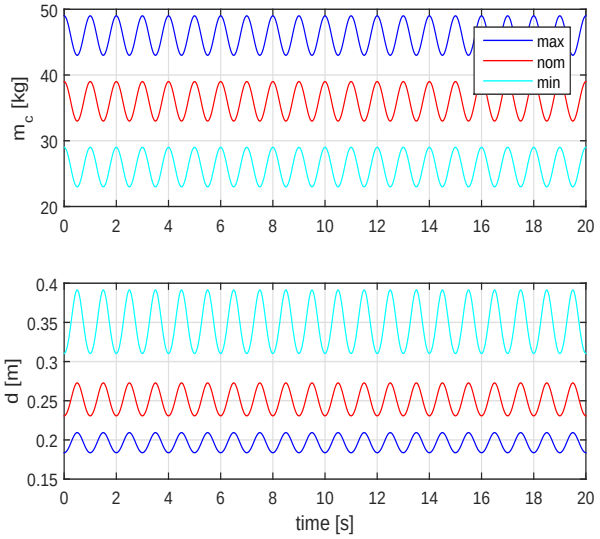

Figure 4.2: Changes of m_c and d during motion for symmetric model.

$I_w = 0.015\ kg.m^2$, $I_m = 0.002\ kg.m^2$, $m_w = 1.5\ kg$. The control gains for inverse kinematic controller are selected as $k_l = 0.3$, $k_\psi = 0.4$. The desired distance of human from the point W, l_d is 0.85 m. The generated torques, τ_R and τ_L are bounded with saturation $\mp 3Nm$. 0.2 $N.m$ is given as the constant torque disturbance, τ_d. $K_p = diag(8.5)$, $K_v = diag(6)$ and $K_i = diag(2)$ are the control gains for the PID dynamic controller. $\lambda = 15$ and $k_1 = 3$ are given for the SMC.

Each simulation is performed for three different values of the mass $m_c = (46, 36, 26) + 3\cos(2\pi t)\ kg$, which are defined as maximum, nominal and minimum i-walker mass during motion. The sinusoidal oscillate, $\mp 3\ kg$, is added to the average masses to represent the load changes on the i-walker due to pHWI.

For the symmetric model, the CG distance, d, is on-line computed with respect to the variations of m_c by the following equation

$$d = 0.45\frac{m_f}{m_c} \tag{4.28}$$

where $m_f = 20\ kg$ is the point mass of the support frame without load, and assumed

to be at the distance 0.45 m from the point W. The variations of m_c and the regarding computed d for the symmetric model is given in Fig. 4.2.

For the asymmetric model, two set of parameters are determined based on the users with symmetric and asymmetric gait patterns, respectively. We assume that the point of the total vertical forces is sliding the y-axis of the body fixed frame. Thus, the parameter β for the asymmetric model shows sinusoidal oscillation and on-line computed based on the distance between the point of the total applied force and the point W. This distance is oscillate as $\mp 0.05\ m$ around zero and $+0.01\ m$ for the users with symmetric and asymmetric gait patterns, respectively. The variations of the related parameters during walking are given in Fig. 4.11.

The parameters of the controllers for the symmetric model are fixed for the mass, $m_c = 36\ kg$. For asymmetric model two cases are considered. The parameters of controller designed for the user with symmetric gait pattern are determined for $m_c = 36\ kg$, $\beta = 0$. For the user with asymmetric gait pattern, the parameters are determined as $m_c = 36\ kg$, $\beta = 0.176\ rad$ and $d = 0.254\ m$.

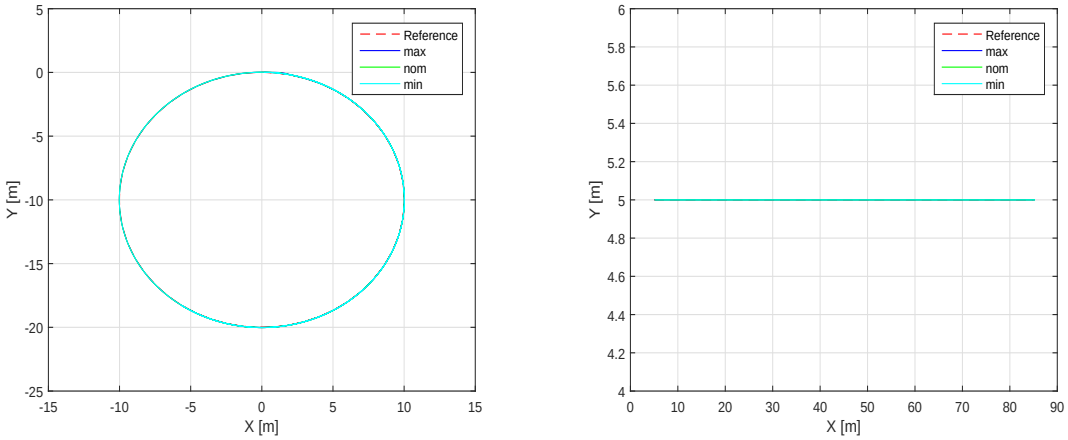

(a) Circle shape trajectory

(b) Straight line trajectory.

Figure 4.3: Motion of PID controlled i-walker for symmetric model.

Two different trajectory is defined for the user to follow.

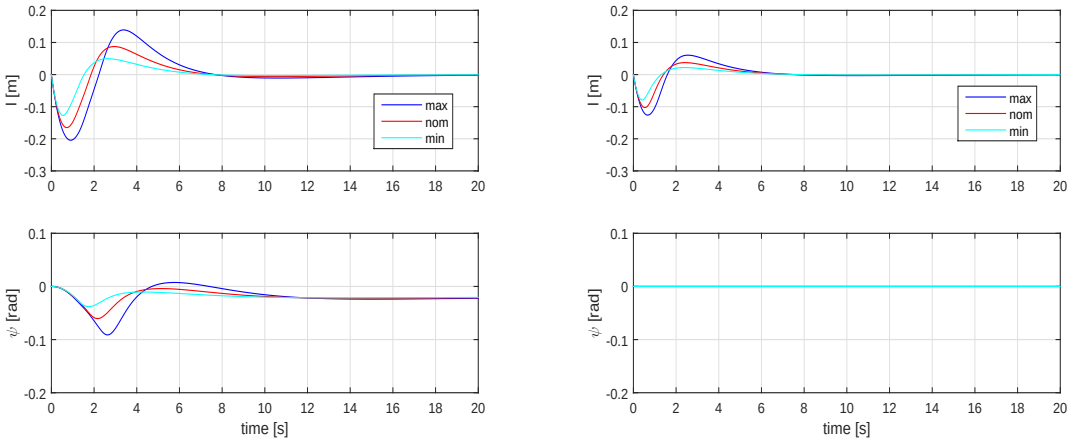

(a) Circle shape trajectory

(b) Straight line trajectory.

Figure 4.4: $\tilde{l}$ and ψ for PID controlled i-walker for symmetric model.

Case 1: The straight path followed by human is planned by

$$\begin{aligned} x_h &= v_h t + c, \\ y_h &= c, \end{aligned} \tag{4.29}$$

where c is constant. The velocities of the planned path is obtained by the following equations:

$$\begin{aligned} \dot{x}_h &= v_h, \\ \dot{y}_h &= 0. \end{aligned} \tag{4.30}$$

The path are chosen as $x_h = 0.4t + 5$, $y_h = 5$, $\alpha_h = 0$. The initial conditions for human and walker are given as $(x_{h0}, y_{h0}, \alpha_{h0}) = (5, 5, 0)$ and $(x_{w0}, y_{w0}, \alpha_{w0}) = (5.2, 5, 0)$, respectively.
Case 2: The circle-shape path followed by human is planned by

$$\begin{aligned} x_h &= R\sin(\omega t), \\ y_h &= R\cos(\omega t) - R \end{aligned} \tag{4.31}$$

The velocities of the planned path is obtained by the equations:

$$\begin{aligned} \dot{x}_h &= R\omega\cos(\omega t), \\ \dot{y}_h &= -R\omega\sin(\omega t). \end{aligned} \tag{4.32}$$

The circle-shape trajectory is defined as $x_h = 10\sin(0.05t)$ and $y_h = 10\cos(0.05t) - 10$. The initial conditions for human and walker are chosen as $(x_{h0}, y_{h0}, \alpha_{h0}) = (0, 0, 0)$ and $(x_{w0}, y_{w0}, \alpha_{w0}) = (0, 0.2, 0)$, respectively.

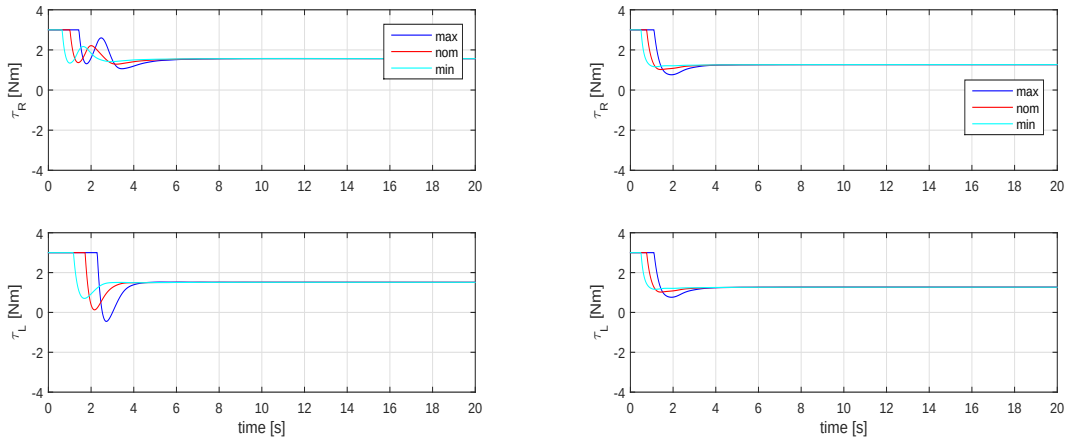

(a) Circle shape trajectory

(b) Straight line trajectory.

Figure 4.5: I-walker control torques of PID for symmetric model.

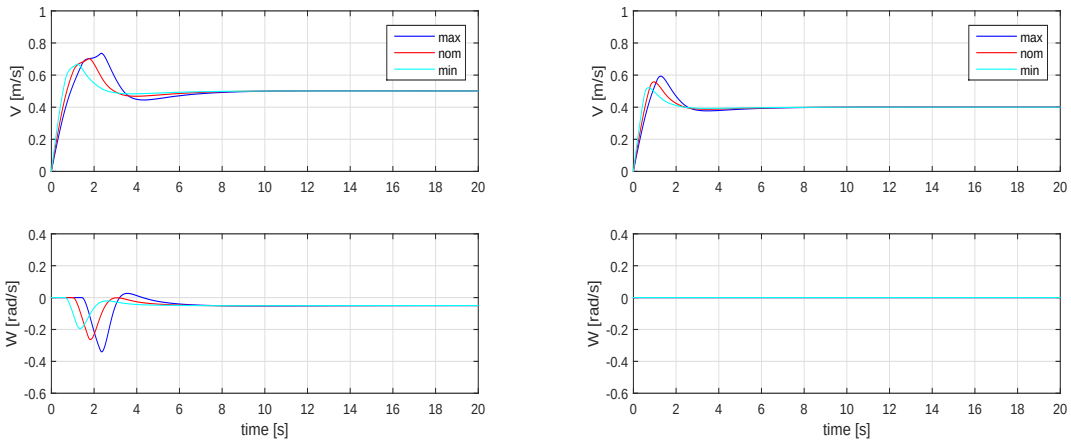

(a) Circle shape trajectory (b) Straight line trajectory.

Figure 4.6: I-walker velocities of PID for symmetric model.

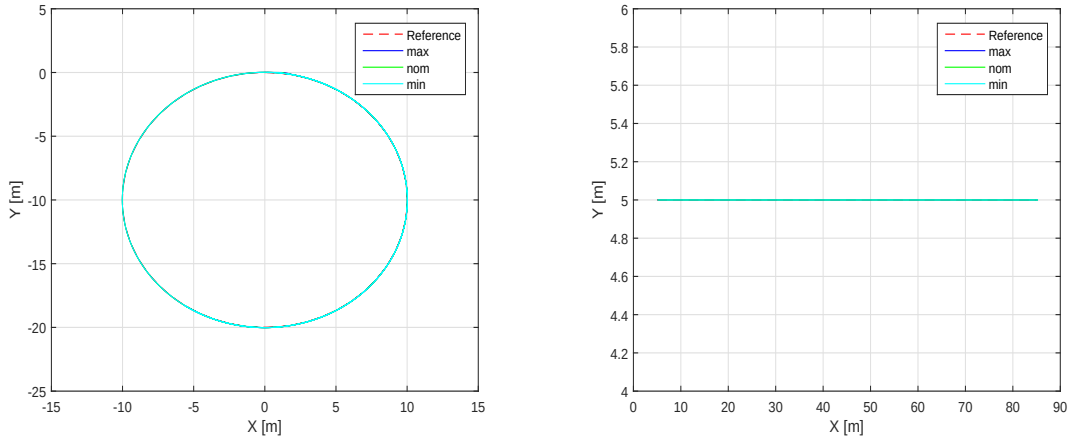

(a) Circle shape trajectory (b) Straight line trajectory.

Figure 4.7: Motion of SMC controlled i-walker for symmetric model.

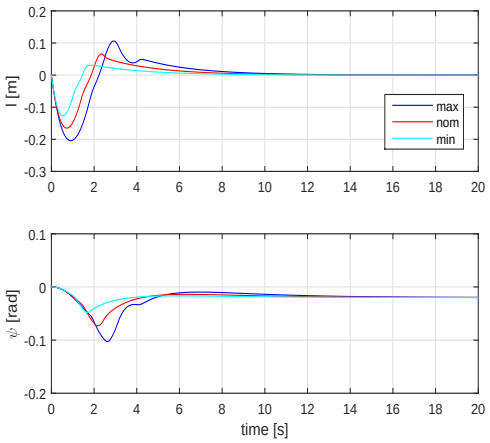

(a) Circle shape trajectory

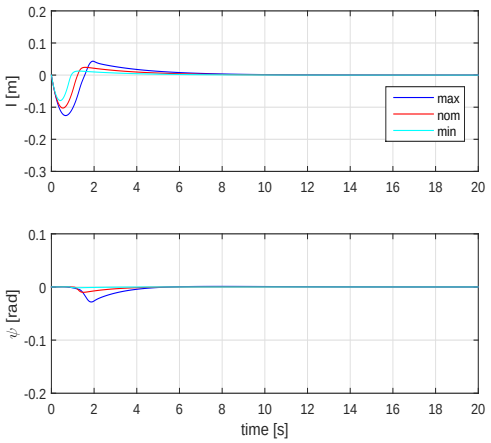

(b) Straight line trajectory.

Figure 4.8: $\tilde{l}$ and ψ for SMC controlled i-walker for symmetric model.

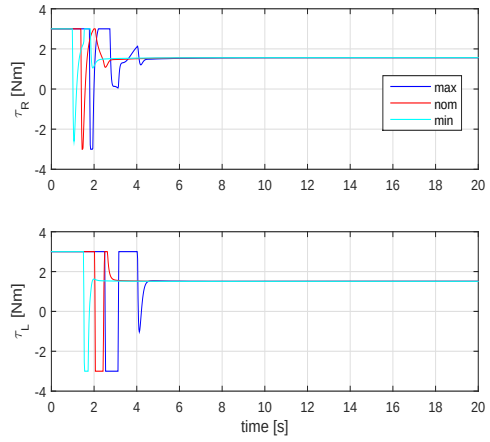

(a) Circle shape trajectory

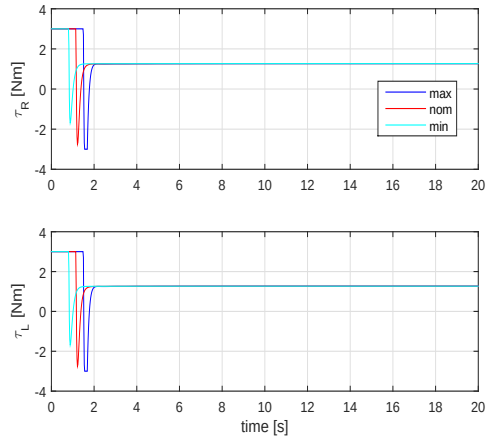

(b) Straight line trajectory.

Figure 4.9: I-walker control torques of SMC for symmetric model.

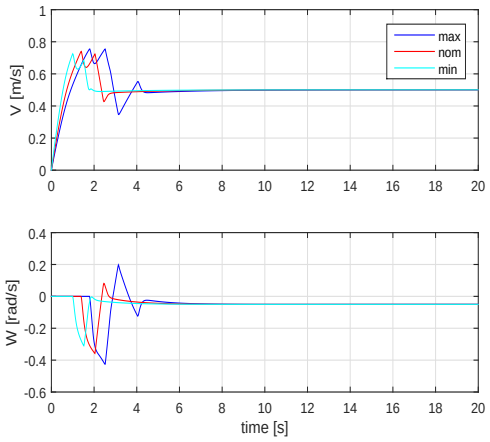

(a) Circle shape trajectory

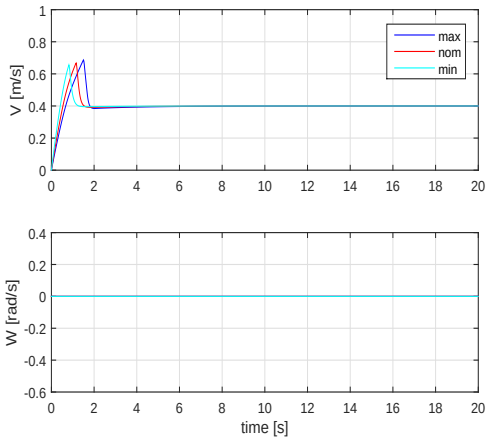

(b) Straight line trajectory.

Figure 4.10: I-walker velocities of SMC for symmetric model.

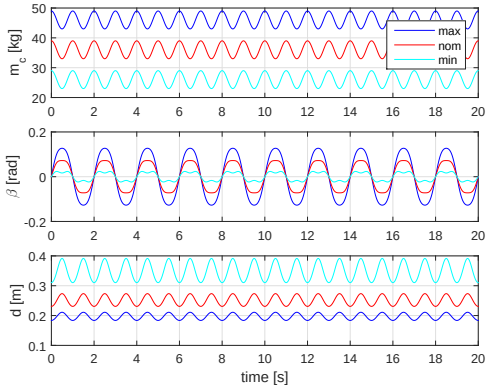

(a) User with symmetric gait pattern.

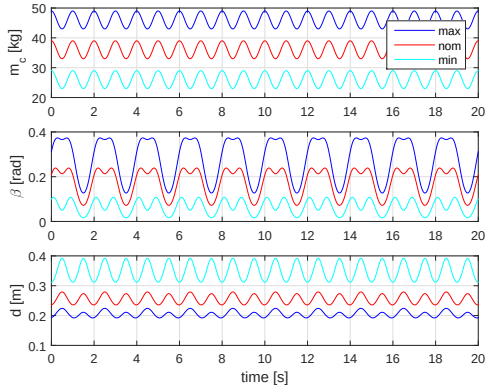

(b) User with asymmetric gait pattern.

Figure 4.11: m_c, β, and d for each type of user.

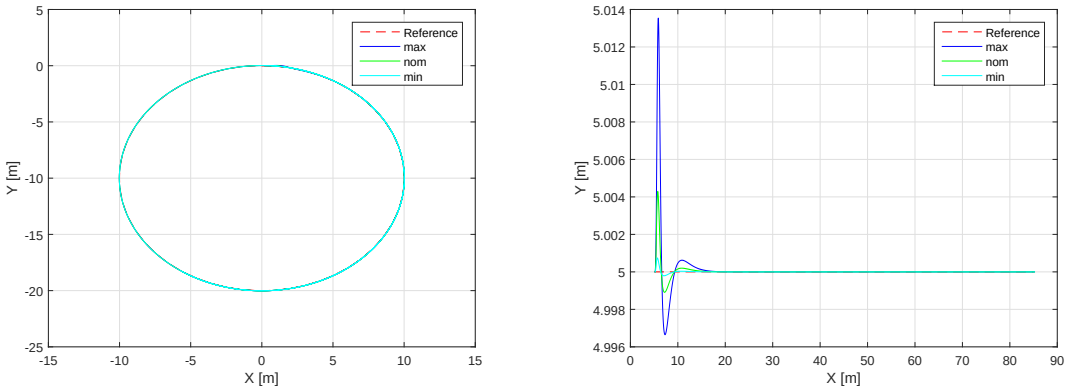

(a) Circle shape trajectory. (b) Straight line trajectory.

Figure 4.12: Motion of PID controlled i-walker with the users having symmetric gait patterns.

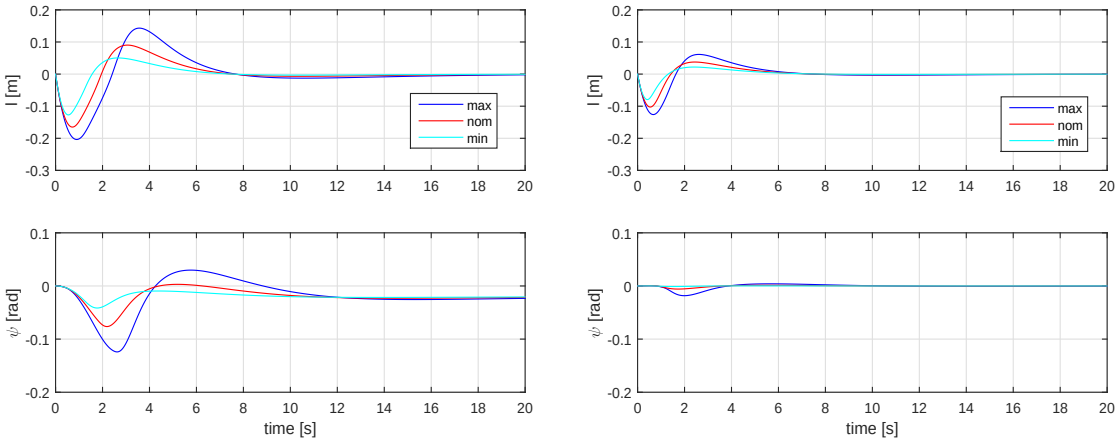

(a) Circle shape trajectory. (b) Straight line trajectory .

Figure 4.13: $\tilde{l}$ and ψ for different trajectories with PID controlled i-walker with the users having symmetric gait patterns.

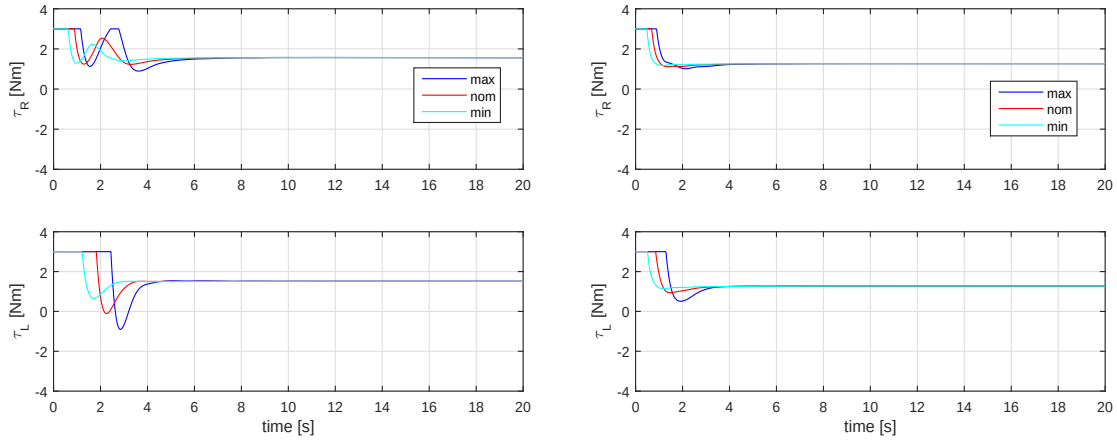

(a) Circle shape trajectory. (b) Straight line trajectory.

Figure 4.14: τ_R and τ_L for PID controlled i-walker with the users having symmetric gait patterns.

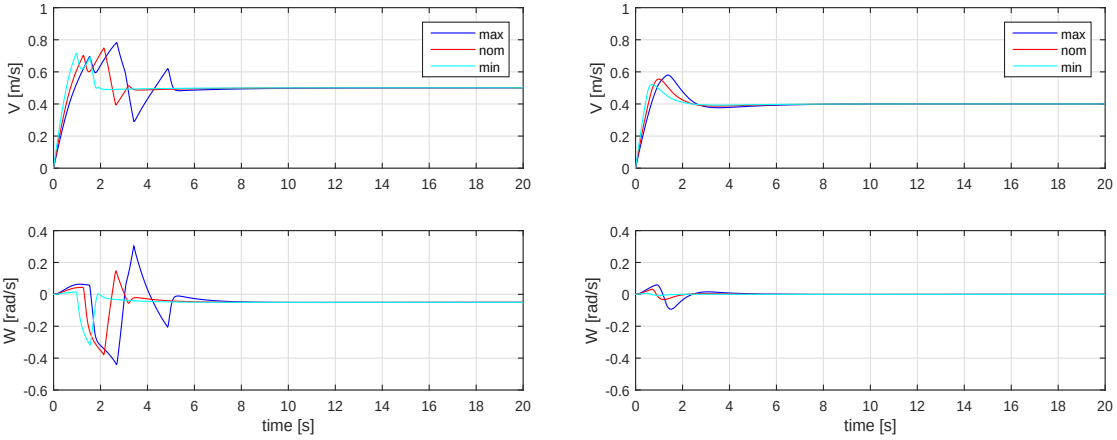

(a) Circle shape trajectory. (b) Straight line trajectory.

Figure 4.15: v_w and ω_w for PID controlled i-walker with the users having symmetric gait patterns.

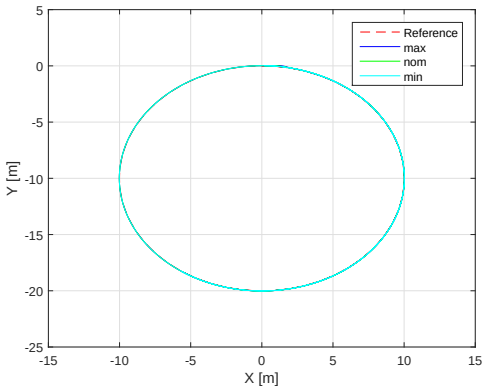

(a) Circle shape human trajectory tracking with SMC controller.

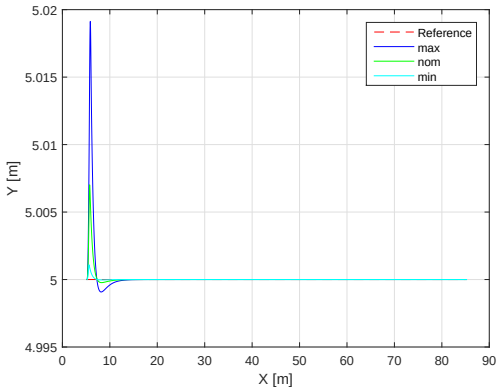

(b) Straight line human trajectory tracking with SMC controller.

Figure 4.16: Motion of SMC controlled i-walker with the users having symmetric gait patterns.

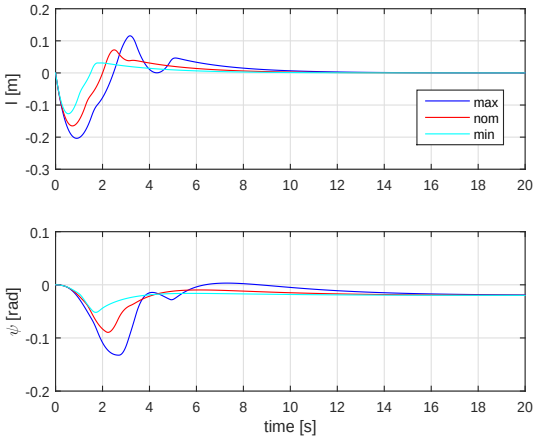

(a) Circle shape trajectory.

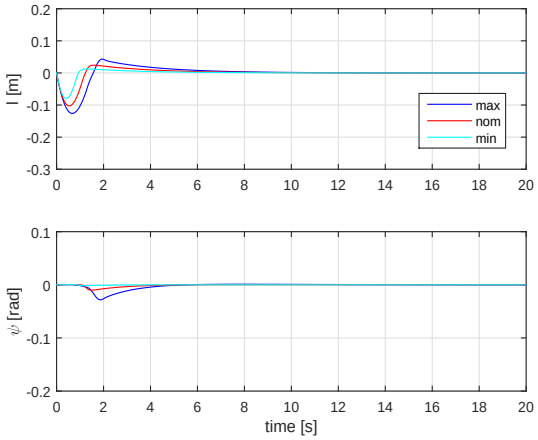

(b) Straight line trajectory .

Figure 4.17: $\tilde{l}$ and ψ for different trajectories with SMC controlled i-walker with the users having symmetric gait patterns.

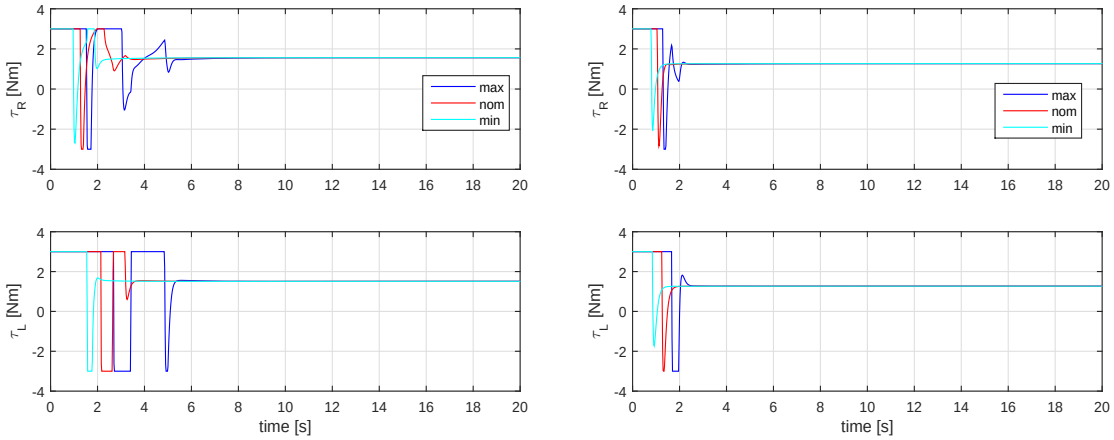

(a) Circle shape trajectory. (b) Straight line trajectory.

Figure 4.18: τ_R and τ_L for SMC controlled i-walker with the users having symmetric gait patterns.

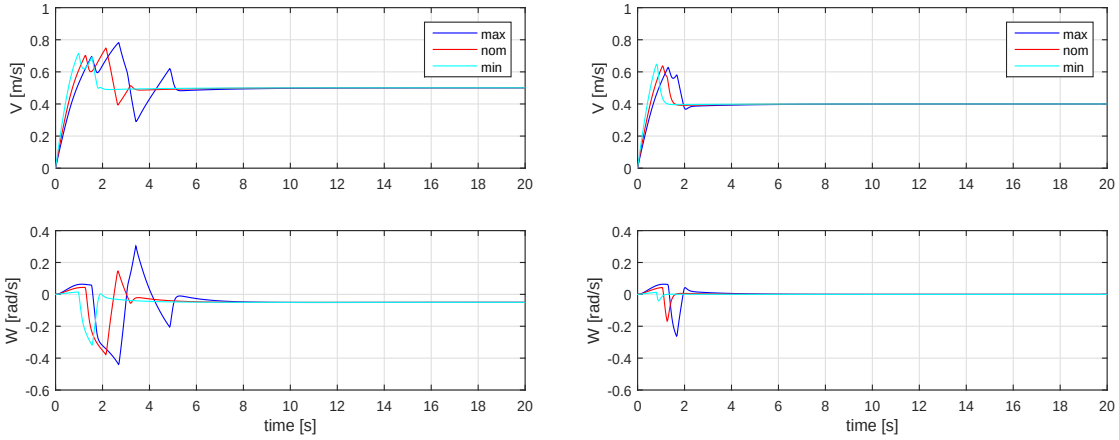

(a) Circle shape trajectory. (b) Straight line trajectory.

Figure 4.19: v_w and ω_w for SMC controlled i-walker with the users having symmetric gait patterns.

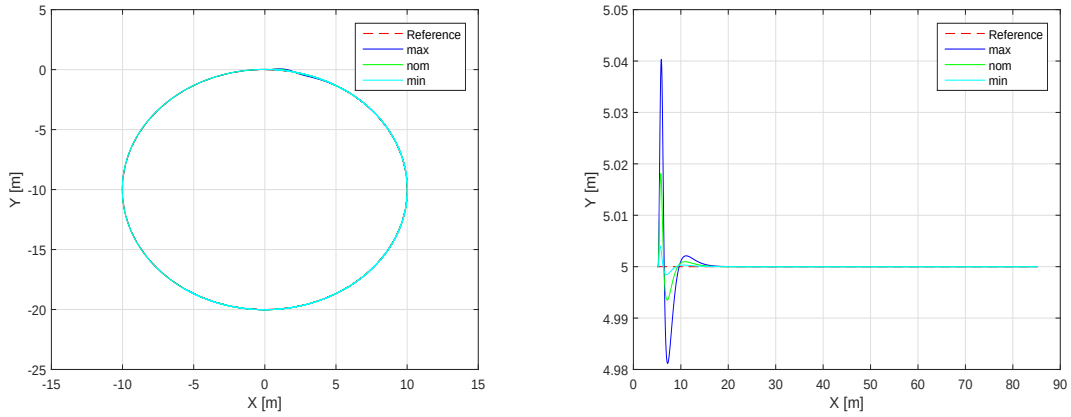

(a) Circle shape trajectory. (b) Straight line trajectory.

Figure 4.20: Motion of PID controlled i-walker with the users having asymmetric gait.

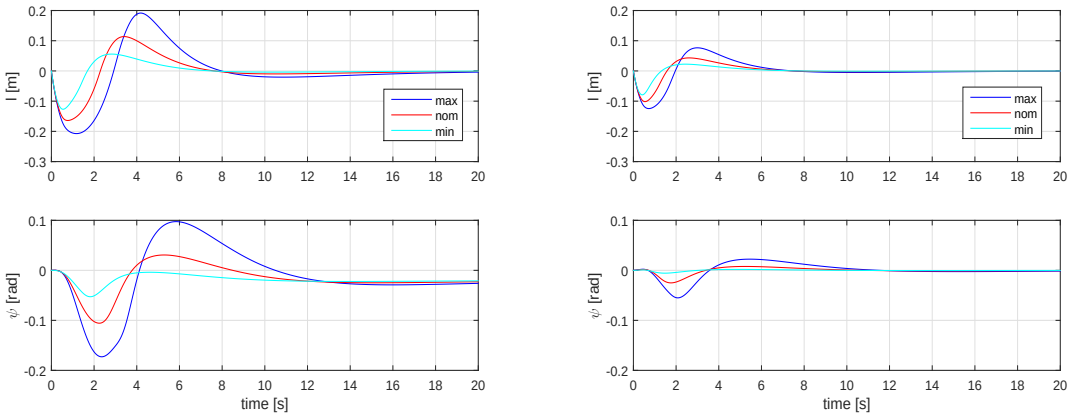

(a) Circle shape trajectory. (b) Straight line trajectory.

Figure 4.21: $\tilde{l}$ and ψ for PID controlled i-walker with the users having asymmetric gait.

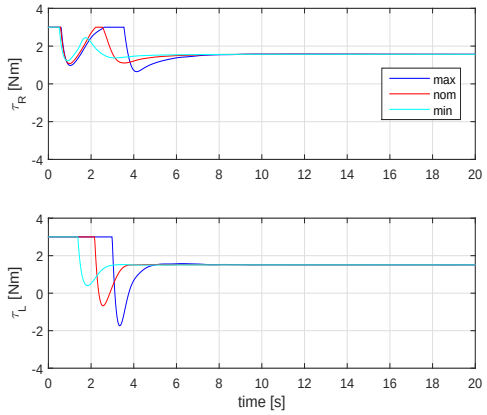

(a) Circle shape trajectory.

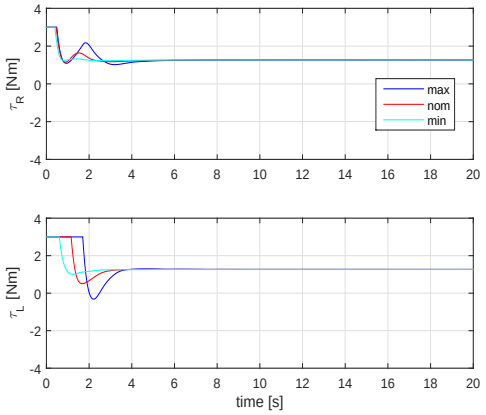

(b) Straight line trajectory.

Figure 4.22: τ_R and τ_L for PID controlled i-walker with the users having asymmetric gait.

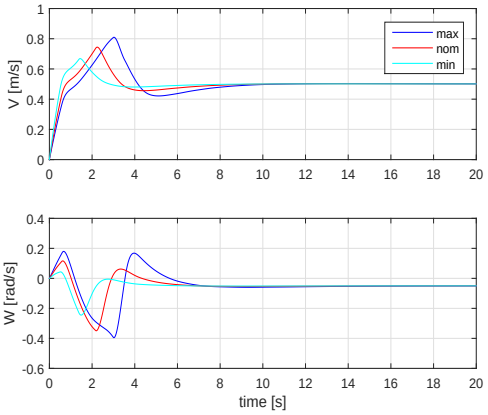

(a) Circle shape trajectory.

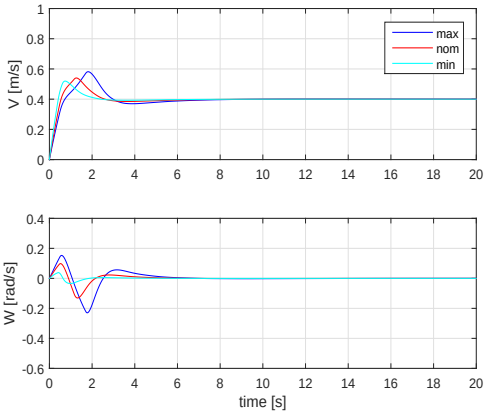

(b) Straight line trajectory.

Figure 4.23: v_w and ω_w for PID controlled i-walker with the users having asymmetric gait.

Simulation results of symmetric model is demonstrated in Figs. 4.3-4.6 for PID and in Figs. 4.7-4.10 for SMC. Asymmetric model is simulated for the users with symmetric and asymmetric gait patterns. Figs. 4.12-4.15 show the PID control results and Figs. 4.16-4.19 display the SMC results for the user with symmetric gait pattern. In addition,

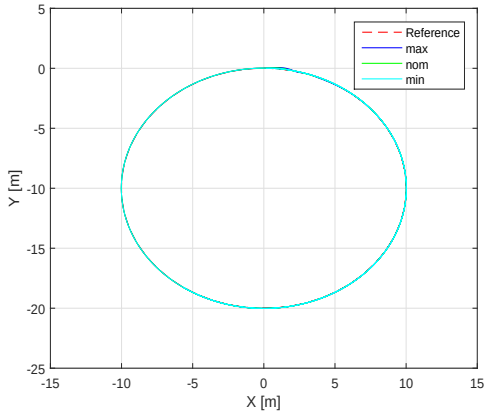

(a) Circle shape trajectory.

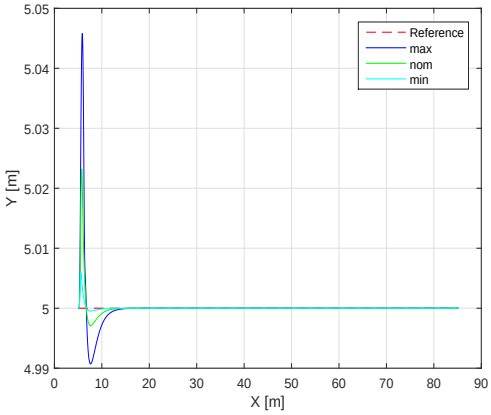

(b) Straight line trajectory.

Figure 4.24: Motion of SMC controlled i-walker with the users having asymmetric gait.

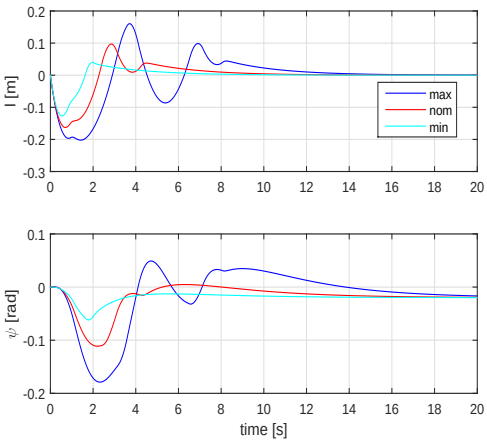

(a) Circle shape trajectory.

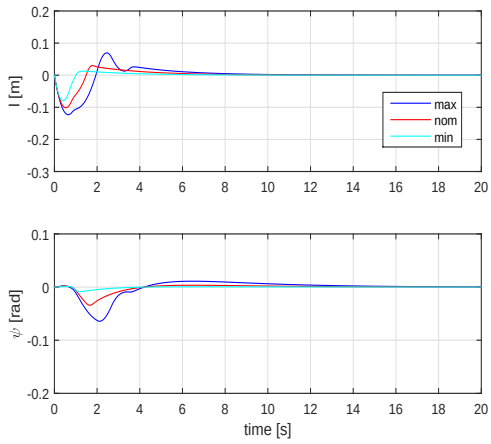

(b) Straight line trajectory.

Figure 4.25: $\tilde{l}$ and ψ for SMC controlled i-walker with the users having asymmetric gait patterns.

Figs. 4.20-4.23 show the PID results and Figs. 4.24-4.27 illustrate the results for SMC for the user with asymmetric gait pattern.

According to simulation results, the stabilization task for the proposed control schemes

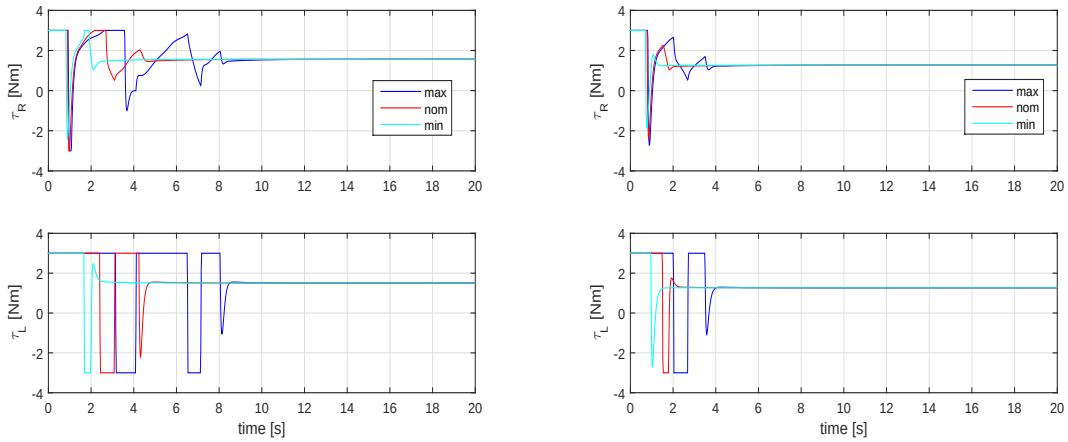

(a) Circle shape trajectory.

(b) Straight line trajectory.

Figure 4.26: τ_R and τ_L for SMC controlled i-walker with the users having asymmetric gait patterns.

is well-achieved. The controller keeps the i-walker in front of the user with desired distance. The stabilization performances of both control schemes show similarity since they are designed based on the feedback linearization technique. However, the applied control torque inputs differentiate from each other in the transient responses. The PID controller have applied smooth control torques, whereas the control torque inputs of SMC have sudden increase and decrease in transient stage. These sudden torque changes are undesirable for the controller performance and the user safety.

In the symmetric model, we have considered that the i-walker CG displacement only occurs along the symmetric axis of the body-fixed frame. This approach could be acceptable for lower load changes on the i-walker to achieve more stable human-walker motion. However, more realistic and comprehensive approach must be that the i-walker CG displacement demonstrates oscillation along the lateral axis as well due to the user gait phase and lateral motion of the user CG. This oscillation is highly dependent on the user weight, body pose, and gait characteristics. To include this lateral CG displacement, we have developed asymmetric model.

The control oriented models above have been developed considering the vertical force

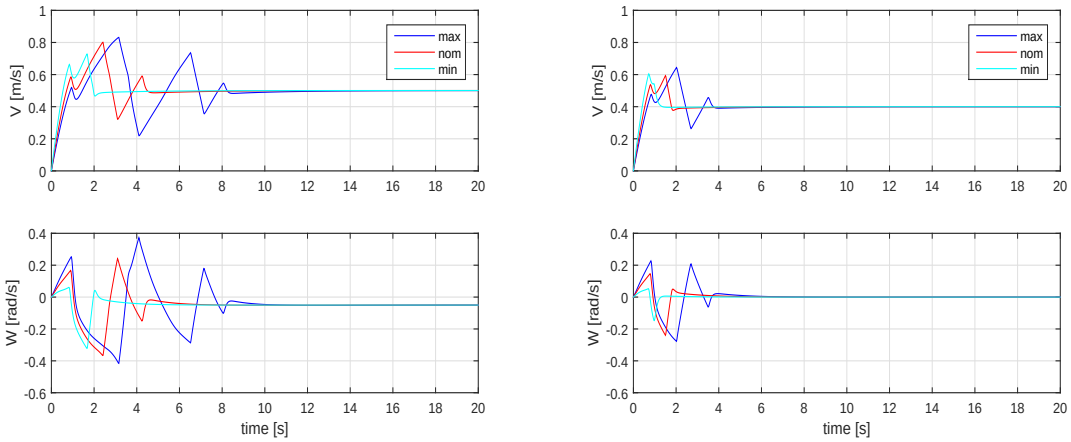

(a) Circle shape trajectory.

(b) Straight line trajectory.

Figure 4.27: v_w and ω_w for SMC controlled i-walker with the users having asymmetric gait patterns.

component of the pHWI. These models have been simulated for the motion of the i-walker human system based on the human motion intention. To cover the horizontal force component of pHWI, we proposed the high-fidelity model making some assumptions. The developed realistic model could be used for the simulation of the i-walker guided human-walker systems.

Chapter 5

Instrumentation

The performance of designed controllers in the previous chapter is highly dependant on the measurement accuracy and resolution. In this chapter, instrumentation is performed in three categories. First, the sensors are selected in adequate resolution and embedded to the suitable places to feed the controllers with required data such that the user can move with the i-walker in a safety way. Second, easily controllable actuator selection is done to achieve the desired torques. Lastly, a processor is chosen so that it can communicate with the other hardware. Block diagram of the overall instrumentation system is shown in Fig. 5.1.

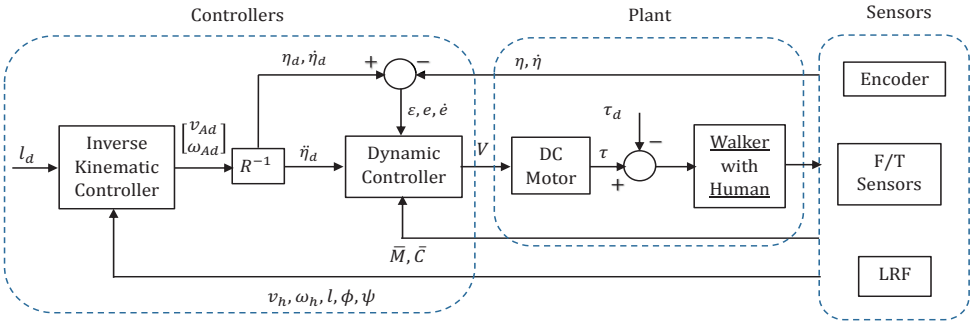

Figure 5.1: Overall system block diagram.

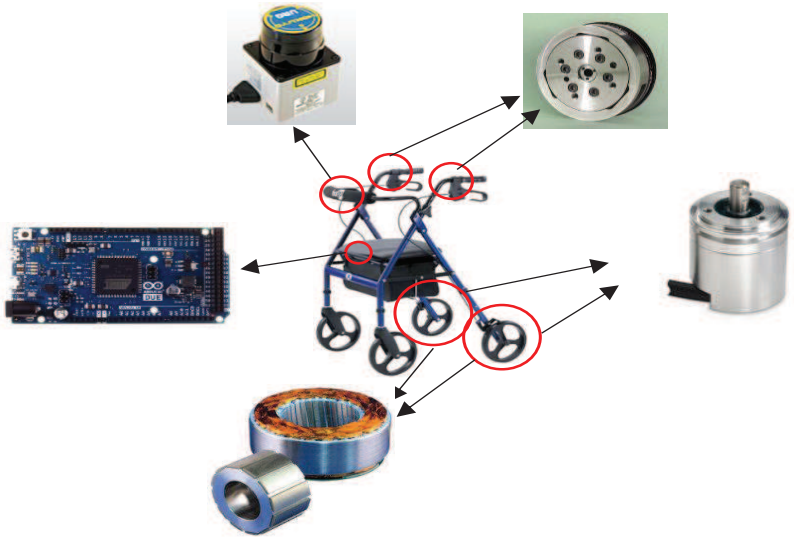

Figure 5.2: Hardware placement.

5.1 Sensors

This section is dedicated to the sensor selection for feeding the designed controllers and monitoring the human gait parameters.

5.1.1 Force/Torque Sensors

The proposed dynamic model controllers are designed based on the location of human-walker CG and the mass of walker with human effect, which is crucial to generate appropriate torques for safe and efficient human-walker mobility. To obtain these information, Force/Torque Sensors (F/T Sensors) is used. The sensors are mounted on the handles in this study and responsible to obtain torque data about X-axis applied by human on the handles. The data is used to figure out the force distribution applied by user on the i-walker during walking. Thus, the force distribution between the handles allows us to estimate the CG place of i-walker system and diagnose whether the user has symmetric

gait or not. Moreover, the combination of the data from F/T sensors and encoders enable to detect some gait parameters, including step and stride lengths, cadence, and the gait events, initial contact and toe off. Thus, the user activity performance can be continuously monitored without any nursing care service.

Figure 5.3: Force/Torque sensor Delta IP60 from ATI Industrial Automation[39].

The maximum torque load is determined according to the following conditions;

• the user have the maximum mass of 130 kg.

• the maximum weight support yielded by the i-walker is twenty percent of the user body weight.

• the distance from the applied force by the user to the F/T sensor is 20 cm.

• the amount of force applied on one handle can be two times as much as the force on the other during walking.

Based on the required maximum torque load above, the Delta IP60 F/T transducers, shown in Fig. 5.3, are selected and mounted between support frame and the handles. The Delta F/T sensor has torque measure range of up to 60 Nm around all axes and the torque resolution of 0.0075 Nm. Since the transducer provides much more powerful signal than the conventional ones, it is robust to noisy environments. The sensor houses a Net F/T system which allows the communication between microcontroller and sensors via the CAN bus or RS485 communication interface.

5.1.2 Laser Range Finder

Laser Range Finder (LRF) gives the location of a detected object in terms of polar coordinates. In this thesis, this sensor is used with a transitions detection algorithm which detects left side (B_L) and right side (B_R) of the user trunk. Then, the distances , l_L and l_R, of these sides to the LRF sensor and the angles, α_L and α_R, between these position vectors and the longitudinal axis of the i-walker are continuously measured, as shown in Fig. 5.4.

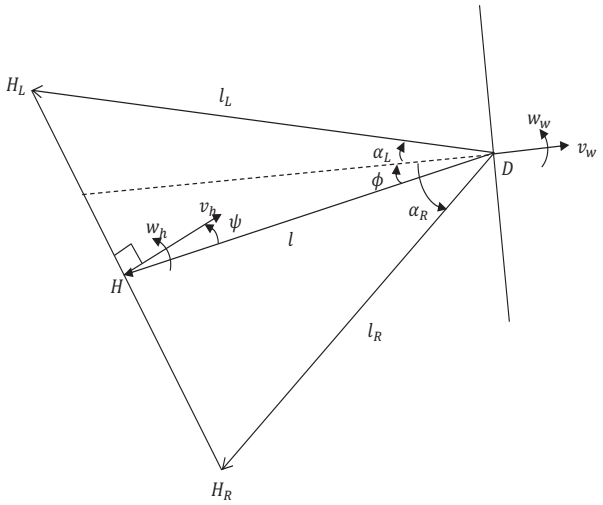

Figure 5.4: Proposed calculation method

However, the presented inverse kinematic controller in (4.2) continuously requires ω_h, v_h, l, ψ, and ϕ which refer to the human angular velocity, the human linear velocity, the distance from LRF sensor to the mid point of human trunk, the angle between l and the longitudinal axis of body fixed frame, and the angle v_h and l, respectively. To this end, the parameters, l, ψ, and ϕ could be computed on-line using cosine theorem and the equality, $\overline{HH_L} = \overline{HH_R}$. The derivatives of these three parameters also obtained since the measurement performs every 100 ms. The other two parameters, w_h and v_h are computed using kinematic relations in (3.11).

Since these two variables, l and ϕ , are time dependent, their derivatives can be taken to compute rate of change. In this thesis, a new method is presented to measure all these

Figure 5.5: Laser range finder URG-04LX [40]

parameters using only an LRF data and encoders data, which does not require the use of wearable sensors like Inertia Measurement Units. The LRF provide the position distance in polar coordinates.

The Laser Range Finder (URG-04LX) is selected for this project, as depicted in Fig 5.5. It is assumed to be mounted on the front of the i-walker at point D. It has a detectable range from 20 mm to 4000 mm and 1 mm resolution. The operation voltage and the scanning area is 5V, 240^o, respectively. The locations of upper body left end and right end is measured each 100 ms. The connection between the computer and the LRF is established with a serial interface (RS-232).

5.1.3 Rotary Magnetic Shaft Encoders

The proposed dynamic controllers (4.10) are directly fed by the position and velocity data of the wheels, whereas the kinematic controller (4.2) uses the walker linear and angular velocities which are computed by (3.2). The wheel angular positions is directly measured by rotary magnetic encoders mounted on the shafts of the rear wheels, while the wheel velocities can be obtained by differentiation of the position signal instead of using another sensor like tachometer. However, when the position signal is noisy, the differentiation process increases the noise in the velocity signal [41]. Thus, absolute encoders could be more reliable for accuracy of the position and velocity data since they are immune to noise.

Figure 5.6: AHM3 magnetic shaft encoder from BEI Sensors [42]

The AHM3 rotary magnetic shaft encoder, as shown in Fig. 5.6, is selected for each rear wheel. The encoder is absolute and outputs 12 bits natural binary codes (i.e. 4096 positions per revolution). The encoders requires minimum 5 V input voltage and communicates with the serial interface CANopen.

5.2 Actuators

The i-walker has a 2 DOF non-holonomic mobile platform. Therefore two independent actuators are necessary to control the i-walker in order to maintain human-walker cooperation. The main criteria of actuator selection in this thesis is performed based on the emergency situation which requires the highest amount of torque. To this end, a *sudden stop* case is defined as the emergency situation for avoiding a collision or preventing a falling.

The maximum torque load is determined with respect to the following assumptions;

1) The user has 130 kg of mass and 0.5 m/s of gait speed during walking with the i-walker.

2) The mass of i-walker frame is 20 kg.

3) The user and i-walker should be stopped within 1 *sec* on sudden stop case.

4) The torque load for each motor could be different at the sudden stop situation since the user may be at single support or double support phase.

5.2.1 Brushless DC Motors

Once the required maximum torque load is determined for each actuator, we decided to use direct drive motors which have no transmission systems, such as belt, chain or gear. Therefore, these motors have less moving parts and less friction than geared motors have, which improves the mechanical performance, motor lifetime, and reduces the operation stiffness and noise.

Figure 5.7: HT03005 brushless DC motor from Allied Motion Technologies Inc. [43]

Two brushless DC motors (HT03005) are chosen from Allied Motion Technologies Inc., as shown in Fig. to drive the i-walker system. The detailed specifications of the selected DC motors are presented in Table 5.1.

Table 5.1: Motor Characteristics.

Variable	Description	Value	Unit
V_p	Design voltage	24	V
T_C	Maximum continuous stall torque	2.01	$N.m$
T_p	Peak torque, 25%	11.4	$N.m$
I_p	Peak current, 15%	42.5	A
S_{NL}	No load speed	89	rad/s
R_m	Terminal resistance, 12%	0.56	Ω
L_m	Terminal inductance, 30%	1.12	mH
K_m	Motor constant	0.36	$(N.m)/\sqrt{W}$
K_t	Torque constant, 10%	0.26	$N.m/A$
K_b	Back EMF constant	0.26	$V/rad/s$
m_m	Motor mass	1.55	kg
b_m	Viscous damping	$5.2\ 10^{-5}$	$N.m/rad/s$
I_m	Rotor inertia	$1.9\ 10^{-4}$	$kg.m^2$

5.3 Processor

In this section, an adequate microcontroller is selected for the high speed data processing in order to smoothly control the i-walker system. The selected microcontroller must have the capability to communicate with all hardware and be able to perform fast mathematical computation for control algorithms.

5.3.1 Microcontroller Board

The Arduino Due shown in Fig. 5.8 is chosen as a microcontroller board to be able to communicate with the selected actuators and sensors. The board is based on a 32 bit ARM core processor, Atmel SAM3X8E ARM Cortex-M3 CPU and runs at 84 MHz. It has a high-speed CAN interface. There are 54 digital input/output pins (12 PWM channels), 12 analog inputs, 2 DAC (digital to analog), an SPI header, an USB OTG capable connection.

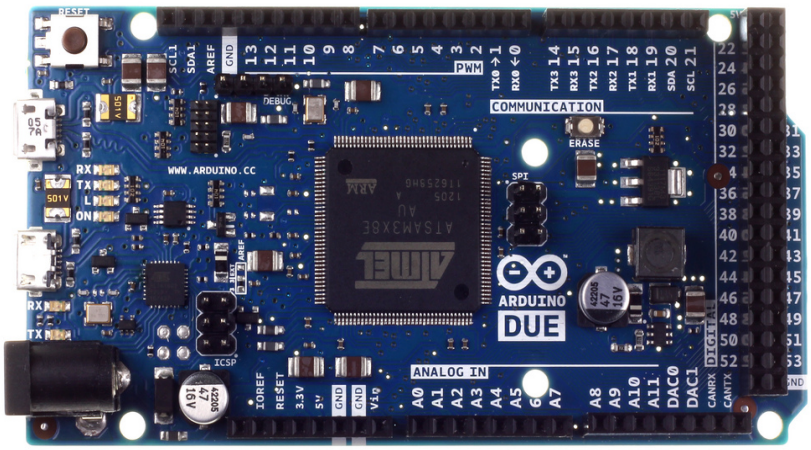

Figure 5.8: The microcontroller board Arduino Due from ARDUINO [44]

The board is operating at 5 V and compatible with all Arduino shields operating at 3.3 V. The controller has a flash memory of 512 KB, 96 KB of RAM.

Chapter 6

Conclusion and Future Work

This thesis has studied kinematic and dynamic modelling, control, and instrumentation of active type i-walkers. Three dynamic models have been developed; two different models with single body dynamics for control design purpose and one high-fidelity model for simulation testing of i-walker guided systems. The pHWI based on the user gait dynamics is considered for all dynamic models. The single-body dynamic models have been classified as symmetric and asymmetric based on the CG displacements of the i-walker system due to pHWI. In the single-body dynamic models, the vertical force components on the i-walker due to pHWI are considered. Then, a high-fidelity model based on the articulated frame steering vehicles has been developed to include the horizontal force components of pHWI. This model has also been designed for the simulation purpose of the i-walker guided systems. Based on the proposed symmetric and asymmetric models, two motion control schemes have been designed. The proposed control schemes consist of an inverse kinematic controller and a nonlinear dynamic controller. The kinematic controller uses the two-body kinematic model and is applied to achieve the required i-walker velocities based on the user relative motion, describing the user motion intention. The dynamic controller has been for torque generation based on two different methods: PID control and SMC. The proposed system models and control schemes have been simulation tested in MATLAB/Simulink environment. The results demonstrate the effectiveness of the proposed system models and control designs. Finally, a human motion detection technique is proposed, and instru-

mentation is performed based on the designed controllers and the measurement technique.

In this study, the controllers for asymmetric dynamic model have been designed assuming a priori knowledge of the user gait parameters. In practice, the corresponding information is not available due to noise and delay in sensing signals. Future work will focus on the implementation of the designed controllers for the user whose gait characteristics are known. Then, the controllers will be generalized for the use with unknown gait characteristics. In the generalization, on-line parameter identification and adaptive control law will be utilized.

Appendix

The entries of the matrix M in (3.31):

$$
\begin{aligned}
M(1,1) &= m_h + m_c + 2m_w \\
M(1,2) &= 0 \\
M(1,3) &= -m_c d \sin(\alpha_w + \beta) \\
M(1,4) &= m_h c \sin\gamma - m_h a \cos\gamma \\
M(1,5) &= M(1,6) = 0 \\
M(2,1) &= 0 \\
M(2,2) &= m_h + m_c + 2m_w \\
M(2,3) &= m_c d \cos(\alpha_w + \beta) \\
M(2,4) &= -m_h c \cos\gamma + m_h a \sin\gamma \\
M(2,5) &= M(2,6) = 0 \\
M(3,1) &= -m_c d \sin(\alpha_w + \beta) \\
M(3,2) &= m_c d \cos(\alpha_w + \beta) \\
M(3,3) &= I_c + m_c d^2 + 2m_w L^2 + 2I_m
\end{aligned}
$$

$$
\begin{aligned}
&M(3,4) = M(3,5) = M(3,6) = 0 \\
&M(4,1) = m_h c \sin\gamma - m_h a \cos\gamma \\
&M(4,2) = -m_h c \cos\gamma + m_h a \sin\gamma \\
&M(4,3) = 0 \\
&M(4,4) = I_h(a^2 + c^2) m_h \\
&M(4,5) = M(4,6) = 0 \\
&M(5,1) = M(5,2) = M(5,3) = M(5,4) = 0 \\
&M(5,5) = I_w \\
&M(5,6) = 0 \\
&M(6,1) = M(6,2) = M(6,3) = M(6,4) = M(6,5) = 0 \\
&M(6,6) = I_w
\end{aligned}
$$

The non-zero entries of the matrix C:

$$
\begin{aligned}
&C(1,3) = -\dot{\alpha}_w m_c d \cos(\alpha_w + \beta) \\
&C(1,4) = -\dot{\gamma}\ (m_h c \sin\gamma - m_h a \sin\gamma) \\
&C(2,3) = -\dot{\alpha}_w m_c d \sin(\alpha_w + \beta) \\
&C(2,4) = -\dot{\gamma}\ (m_h c \cos\gamma + m_h a \cos\gamma)
\end{aligned}
$$

The $A(q)$, $B(q)$ matrices and $R(\dot{q})$, $V(q)$ vectors are

$$
A(q) = \begin{bmatrix}
-\sin\alpha & \cos\alpha & 0 & 0 & 0 & 0 \\
\cos\alpha & \sin\alpha & -L & 0 & -r & 0 \\
\cos\alpha & \sin\alpha & L & 0 & 0 & -r
\end{bmatrix},
$$

$$B(q) = \begin{bmatrix} \cos(\alpha_w - \gamma) & -\sin\gamma & 0 & 0 \\ \sin(\alpha_w - \gamma) & 0 & 0 & 0 \\ 0 & 0 & 0 & 0 \\ (b+c)\cos\gamma & 0 & 0 & 0 \\ 0 & 0 & 1 & 0 \\ 0 & 0 & 0 & 1 \end{bmatrix},$$

$$R(\dot{q}) = \begin{bmatrix} 0 \\ 0 \\ b_R(\dot{\alpha}_w - \dot{\gamma}) \\ -b_R(\dot{\alpha}_w - \dot{\gamma}) \\ b_m\dot{\theta}_R \\ b_m\dot{\theta}_R \end{bmatrix}, \quad V(q) = \begin{bmatrix} 0 \\ 0 \\ k_R(\alpha_w - \gamma) \\ -k_R(\alpha_w - \gamma) \\ 0 \\ 0 \end{bmatrix}.$$

Bibliography

[1] L. B. Bolton, C. A. Gassert, and P. F. Cipriano, "Smart technology, enduring solutions: Technology solutions can make nursing care safer and more efficient," *American Academy of Nursing*, vol. 22, no. 4, 2008

[2] N. Costa and D. G. Caldwell, "Control of a biomimetic soft-actuated 10dof lower body exoskeleton," *IEEE/RAS-EMBS International Conference on Biomedical Robotics and Biomechatronics*, pp. 495-501, Feb. 2006

[3] O. Chuy, Y. Hirata, Z. Wang, and K. Kosuge, "Approach in assisting a sit-to-stand movement using robotic walking support system, *IEEE/RSJ International Conference on Intelligent Robots and Systems*, pp. 4343-4348, Oct. 2006

[4] G. Lee, E.-J. Jung, T. Ohnuma, N. Y. Chong, and B.-J. Yi, "JAIST robotic walker control based on a two-layered Kalman filter, *IEEE International Conference on Robotics and Automation*, pp. 3682-3687, May 2011

[5] Y. Hirata, A. Muraki, and K. Kosuge, "Motion control of intelligent passive-type walker for fall-prevention function based on estimation of user state, *IEEE International Conference on Robotics and Automation*, pp. 3498-3503, May 2006

[6] S. Dubowsky, F. Genot, S. Godding, H. Kozono, A. Skwersky, H. Yu, and L. S. Yu, "PAMM - a robotic aid to the elderly for mobility assistance and monitoring: a helping-hand for the elderly, *IEEE International Conference on Robotics and Automation*, vol. 1, pp. 570-576, Apr. 2000

[7] Y. Hirata, A. Hara, and K. Kosuge, "Motion control of passive intelligent walker using servo brakes," *IEEE Transactions on Robotics*, vol. 23, issue. 5, pp. 981-990, Oct. 2007

[8] Y. Hirata, C. Oscar Jr, A. Hara, and K. Kosuge, "Human adaptive motion control of active and passive type walking support system," *IEEE Workshop on Advanced Robotics and its Social Impacts*, pp. 139-144, Jun. 2005

[9] C. H. Ko, K. Young, Y. Huang, and S. K. Agrawal, "Active and passive control of walk-assist robot for outdoor guidance," *IEEE/ASME Transactions on Mechatronics*, vol.18, no.3, pp.1211-1220, Jun. 2013

[10] Y. Hirata, A. Muraki, and K. Kosuge, "Motion control of intelligent walker based on renew of estimation parameters for user state," *IEEE/RSJ International Conference on Intelligent Robots and Systems*, pp. 1050-1055, Oct. 2006

[11] J. Y. Tung, W. H. Gage, P. Poupart, and W. E. McIlroy, "Upper limb contributions to frontal plane balance control in rollator-assisted walking," *Assistive Technology: The Official Journal of RESNA* , vol. 26:1, pp. 15-21, 2014

[12] M. Alwana, A. Ledoux, G. Wasson, P. Sheth, C. Huang, "Basic walker-assisted gait characteristics derived from forces and moments exerted on the walkers handles: results on normal subjects," *Medical Engineering & Physics*, vol. 29, no. 3, pp. 380-389, Apr. 2007

[13] A. Abellanas, A. Frizera, R. Ceres, J. A. Gallego "Estimation of gait parameters by measuring upper limbwalker interaction forces," *Sensors and Actuators A: Physical*, vol. 162, no. 2, pp. 276-283, Aug. 2010

[14] C. A. Cifuentes, C. Rodriguez, A. Frizera, and T. Bastos "Sensor fusion to control a robotic walker based on upper-limbs reaction forces and gait kinematics," *2014 5th IEEE RAS & EMBS International Conference on Biomedical Robotics and Biomechatronics* , pp. 1098-1103, Aug. 2014

[15] D. Levine, J. Richards, and M. W. Whittle, *Whittle's Gait Analysis*, Churchill Livingstone, 2012

[16] P. A. Houglum, D. B. Bertoti, *Brunnstrom's Clinical Kinesiology*, F.A. Davis Company, Philadelphia, 2012

[17] A. Silva Jr., and F. Sup, "Design and control of a two-wheeled robotic walker for balance enhancement," *IEEE International Conference on Rehabilitation Robotics*, pp. 1-6, 2013

[18] Y. N. Wang, S. Y. Wang, R. P. Tan, Y. L. Jiang, K. Ishida, and M. G. Fujie, "Adaptive control method for a walking support machine considering center-of-gravity shifts and load changes," *IEEE International Conference on Advanced Mechatronic Systems*, pp. 684-689, Sept. 2012

[19] R. P. Tan, S. Y. Wang, Y. L. Jiang, T. Chai, K. Ishida, and M. G. Fujie, "Adaptive controller for omni-directional walker: improvement of dynamic model," *IEEE International Conference on Mechatronics and Automation*, pp. 325-330, Aug. 2011

[20] R. P. Tan, S. Y. Wang, Y. L. Jiang, K. Ishida, and M. G. Fujie, "Motion control of omni-directional walker for walking support," *IEEE/ICME International Conference on Complex Medical Engineering*, pp. 633-636, May. 2011

[21] Fall Guys Research Lab, Research on falls and more, *http://fallguysresearchlab.com/for-patientsfamilies/*

[22] T. Fukao, H. Nakagawa, and N. Adachi "Adaptive tracking control of a nonholonomic mobile robot," *IEEE Transaction on Robotics and Automation* , vol. 16, no. 5, pp. 609-615, Oct. 2000

[23] H. Zeng-Guang, Z. An-Min, L. Cheng and M. Tan "Adaptive control of an electrically driven nonholonomic mobile robot via backstepping and fuzzy approach," *IEEE Transactions on Control Systems Technology*, vol. 17, no. 4, pp. 803-815, Jun. 2009

[24] R. Fierro and F. L. Lewis, "Control of a nonholonomic mobile robot: backstepping kinematics into dynamics," *Proc. IEEE Conference on Decision and Control*, vol. 4, pp. 3805-3810, Dec. 1995

[25] T. Albagul, and M. Wahyudi "Dynamic modelling and adaptive traction control for mobile robots," *International Journal of Advanced Robotic Systems*, vol.1, no.3, pp. 149-154, Aug. 2004

[26] R.P.Tan, S.Y.Wang, Y.L.Jiang, K.Ishida, M.G.Fujie, "Motion control of omni-directional walker for walking support," *IEEE/ICME International Conference on Complex Medical Engineering*, 2011

[27] Nasser Lashgarian Azad, Dynamic modelling and stability controller development for articulated steer vehicles, PhD dissertation, University of Waterloo, 2006

[28] D. N. L. Horton and D. A. Crolla, "Theoretical analysis of the steering behaviour of articulated frame steer vehicles," *Vehicle System Dynamics*, vol. 15, no. 4, pp. 211-234, 1986.

[29] Y. Hirata, C. Oscar Jr, A. Hara, K. Kosuge, "Human adaptive motion control of active and passive type walking support system," *IEEE Workshop on Advanced Robotics and its Social Impacts*, 2005

[30] C. Ko, K. Young, Y. Huang, S. Agrawal, "Active and passive control of walk-assist robot for outdoor guidance," *IEEE/ASME Transactions on Mechatronics*, vol. 18, no. 3, 2013

[31] Y. L. Jiang, S. Y. Wang, K. Ishida, T. Ando and M. G. Fujie, "Directional intention identification based on the force interaction between an omnidirectional walker and a human," *ICIC Express Letters, Part B: Applications*, vol. 1, no. 2, pp.195-200, 2010

[32] Y. L. Jiang, S. Y. Wang, K Ishida, T. Ando and M. G. Fujie, "Directional intention identification for running control of an omnidirectional walker," *Journal of Advanced Computational Intelligence and Intelligent Informatics*, vol.14, no.7, pp.784-792, 2010

[33] S. Suzuki, Y. Hirata, and K. Kosuge, "Development of intelligent passive cane controlled by servo brakes," *The 18th IEEE International Symposium on Robot and Human Interactive Communication*, Toyama, Japan, Sept, 2009

[34] C. A. Cifuentes, C. Rodriguez, A. Frizero-Neto, T. F. Bastos-Filho, and R. Carelli, "Multimodal human-robot interaction for walker-assisted gait," *IEEE Systems Journal*, no. 99, pp. 1-11, May. 2014

[35] R. Dhaouadi and A. A. Hatab, "Dynamic modelling of differential-drive mobile robots using lagrange and newton-euler methodologies: A unified framework," *Advances in Robotics and Automation*, vol. 2, Sep. 2013

[36] F. L. Lewis, D. M. Dawson, and C. T. Abdallah, *Robot Manipulator Control Theory and Practice*, CRC Press, 2003

[37] R. M. Murray, Z. Li and S. S. Sastry, *A Mathematical Introduction to Robotic Manipulation*, CRC Press, 1993

[38] J. J. E. Slotine and W. Li, *Applied Nonlinear Control*, Prentice-Hall, Englewood Cliff, New Jersey, 1991

[39] ATI Industrial Automation, http://www.ati-ia.com/products/ft/ft_models.aspx?id=Delta

[40] Hokuyo Automatic Co.,LTD., https://www.hokuyo-aut.jp/02sensor/07scanner/urg_04lx.html

[41] M. Jouaneh, *Fundamentals of Mechatronics*, Cengage Learning, Stamford, Connecticut, USA, 2013

[42] BEI Sensors, http://http://www.beisensors.com/pdfs/ahm3-magnetic-absolute-encoder-canopen_en.pdf

[43] Allied Motion Technologies Inc., http://www.alliedmotion.com/Data/Documents/HT_Series_Torque_Motors_Spec_R3(scrn).pdf

[44] ARDUINO, http://www.arduino.cc/en/Main/arduinoBoardDue